remote sensing

MDPI

Article

Simplified Marsh Response Model (SMRM): A Methodological Approach to Quantify the Evolution of Salt Marshes in a Sea-Level Rise Context

Miguel Inácio [1,2,*], M. Conceição Freitas [1,2], Ana Graça Cunha [1,2], Carlos Antunes [2], Manel Leira [2,3,4], Vera Lopes [1,2], César Andrade [1,2] and Tiago Adrião Silva [5]

1 Departamento de Geologia, Faculdade de Ciências, Universidade de Lisboa, Building C6, Floor 3, Campo Grande, 1749-016 Lisbon, Portugal; cfreitas@fc.ul.pt (M.C.F.); agcunha@fc.ul.pt (A.G.C.); vplopes@fc.ul.pt (V.L.); candrade@fc.ul.pt (C.A.)
2 Instituto Dom Luiz, Faculdade de Ciências, Universidade de Lisboa, Building C6, Floor 3, Campo Grande, 1749-016 Lisbon, Portugal; cmantunes@fc.ul.pt (C.A.); m.leira@udc.es (M.L.)
3 BioCost Research Group, Facultade de Ciencias and Centro de Investigacións Científicas Avanzadas (CICA), Universidade de A Coruña, 15071 Corunha, Spain
4 Biodiversity and Applied Botany Research Group, Departamento de Botánica, Facultade de Bioloxía, Universidade de Santiago de Compostela, 15782 Santiago de Compostela, Spain
5 Department F.-A. Forel for Environmental and Aquatic Sciences, and Institute for Environmental Sciences, University of Geneva, 1205 Geneva, Switzerland; geotsilva@gmail.com
* Correspondence: mfinacio@fc.ul.pt

Abstract: Salt marshes are highly valued coastal environments for different services: coastline protection, biodiversity, and blue carbon. They are vulnerable to climate changes, particularly to sea-level rise. For this reason, it is essential to project the evolution of marsh areas until the end of the century. This work presents a reduced complexity model to quantify salt marshes' evolution in a sea-level rise (SLR) context through combining field and remote sensing data: SMRM (Simplified Marsh Response Model). SMRM is a two-dimensional rule-based model that requires four parameters: a digital terrain model (DTM), local tidal levels, a sea-level rise projection, and accretion rates. A MATLAB script completes the process, and the output is a GeoTIFF file. Two test areas were selected in Tróia sandspit (Setúbal, Portugal). Additionally, a sensitivity analysis for each parameter's influence and a comparison with SLAMM (another rule-based model) were undertaken. The sensitivity analysis indicates that SLR is the most relevant parameter, followed by accretion rates. The comparison of SMRM with SLAMM shows quite similar results for both models. This new model application indicates that the studied salt marshes could be resilient to conservative sea-level rise scenarios but not to more severe sea-level rise projections.

Keywords: accretion rates; reduced-complexity models; remote sensing application; GIS

Citation: Inácio, M.; Freitas, M.C.; Cunha, A.G.; Antunes, C.; Leira, M.; Lopes, V.; Andrade, C.; Silva, T.A. Simplified Marsh Response Model (SMRM): A Methodological Approach to Quantify the Evolution of Salt Marshes in a Sea-Level Rise Context. *Remote Sens.* **2022**, *14*, 3400. https://doi.org/10.3390/rs14143400

Academic Editors: Qiusheng Wu and Dehua Mao

Received: 15 February 2022
Accepted: 12 July 2022
Published: 15 July 2022

1. Introduction

Salt marshes are vegetated intertidal wetlands with high ecological value because of their biodiversity. They are one of the most productive ecosystems of the biosphere [1]. In addition, salt marshes (and mangroves) are widely recognized as playing a significant role in coastal defense due to their ability to dissipate wave energy and temporarily store floodwater. Moreover, they are a key feature for wildlife conservation, carbon sequestration [2], and a significant source of organic material and nutrients essential for marine communities [3]. Some of the earliest conservation reserves were salt marshes [4].

Anthropic pressure over these delicate systems and climate-driven changes in external forcing, may threaten the services these environments provide. Worldwide, vast areas of salt marshes have been converted into agricultural land, industrial use, or port facilities, despite lesser losses to other uses recently [4].

One of the main consequences of present and future climate changes is the sea-level rise (SLR), which may negatively impact these ecosystems and severely threaten estuarine areas [5]. Expected impacts include the destruction of habitats and the reduction of the protection they afford to the adjacent coastline and land. Salt marsh establishment is intrinsically linked to sea-level and tidal oscillations because flooding is the primary mechanism for sediment delivery to the marsh platforms [6]. Sea level and tidal range control immersion time, a parameter to which marsh vegetation is susceptible. Salt marsh areas are also prone to erosion, generally attributed to decreased sediment supply, and increased magnitude and frequency of extreme events. Both drivers are also indirectly influenced by SLR [7].

Remote sensing is essential to project the evolution of wetlands in a climate-change context [8,9], being a rapid and cost-effective method to obtain relevant data [10]. The increasing number of studies that use remote sensing reflects the access to this tool, e.g., [11–14].

Studying the future evolution of wetland environments, including salt marshes, is crucial because their reduction or destruction may increase adverse climate change impacts. For instance, the increase in CO_2 emissions to atmosphere related to wetlands' destruction represents 3–19% of the increase due to deforestation [15]. An increase in CO_2 emissions to the atmosphere is explained by the release of organic carbon sequestered by these environments (known as blue carbon [16]). Furthermore, it is estimated that the carbon stored in European salt marshes represents 4% of all carbon accumulated in coastal areas [17].

Other factors can impact the behavior of these environments in the future. Salt marsh characteristics and dynamics result from complex interactions among hydrodynamics, sediment transport, and biological processes [18]. Changes in salinity, partially dependent on rainfall, affect their stability and local hydrodynamic patterns, ultimately affecting the distribution of accretion rates over different parcels of the salt marsh. Other significant parameters are elevation distribution and accommodation space in the land, neighboring salt marshes. These areas may provide room for landward marsh expansion, which may compensate seaward erosion; thus, maintaining invariance of the total marsh area. In fact, when SLR rates are higher than accretion rates, salt marshes may evolve in space and time following two ways: (1) marsh areas at higher elevations and fringing the coastline will migrate landwards, providing that the three following conditions are met—absence of vertical barriers (avoiding coastal squeeze), existence of accommodation space, and rate of horizontal marsh expansion upland equal or higher than the rate of horizontal progression of the inundation limit; (2) marsh areas at lower elevations will be more frequently flooded, experience larger submersion periods, and are not colonized, or remain colonized by low marsh vegetation [19].

In conceptual terms, if accretion rates closely match SLR rates, salt marshes may grow or maintain their area. However, the acceleration of SLR rates observed recently and projected into the near future suggests that this equilibrium is at risk of being reversed [20]. It is essential to rely on numerical or rule-based models to project and comprehend how salt marshes can evolve until the end of the 21st century. These are powerful predictive tools that incorporate nonlinear feedback between salt marsh ecosystem morphology and sediment transport and deposition processes [21]. Salt marsh evolution models and marsh response to SLR models can be classified as zero-dimensional (a single marsh point within a marsh is modeled), one-dimensional (simulating the evolution of a salt marsh transect), two-dimensional (when applied to a marsh platform), and landscape models (that simulate processes over an entire estuary) [6].

This work aims to present the Simplified Marsh Response Model, which is a rule-based model to quantify the evolution of salt marsh areas until the end of the century, combining remote sensing with data in the field and literature. SMRM considers the balance between SLR and accretion rates. Several models have been proposed recently to project the evolution of these vulnerable environments under a climate-change context [22–25]. Such models assume that many data are readily available (e.g., salinity, precipitation, wind, storm surge, uplift/subsidence, land use, erosion, and waves). However, this is not always

possible (diversity, quality, and quantity of data are common drawbacks), and in many cases, they involve a too high investment regarding the results.

Moreover, the assumption that adding more detail and variables to models always leads to better results is questionable. Adding too many parameters can result in a situation where neither the studied systems nor the model are understandable [26]. In contrast, reduced complexity models are distinguished by a high degree of simplification, incorporating only the fundamental parameters to describe the processes or trends characterizing a particular coastal system at given time and spatial scales, leaving out as many processes as possible [27,28]. The Simplified Marsh Response Model (SMRM) is a reduced-complexity, two-dimensional rule-based model. The motivation to present this simplified model is that the complexity of the coastal systems often challenges the ability of complex models to forecast timely and accurately the meso to macro-scale evolution of marsh environments [29]. SMRM needs only four parameters to run and departs from a digital terrain model (DTM) of the studied marsh area. Using a DTM is the basis for modeling the evolution of salt marshes, a fundamental application of remote sensing to coastal areas. In order to evaluate its performance, SMRM was applied to two test areas in Portugal. The results were compared to those obtained by modeling marsh changes in the same areas for the same period of time with SLAMM (Sea Level Affecting Marsh Model) (Warren Pinnacle Consulting, Inc., Warren, VT, USA; Washington, DC, USA), a more complex rule-based model. In addition, a sensitivity analysis was performed to evaluate the influence of each input parameter on the final results.

2. Test Areas

Almost 50% of Portugal's mainland perimeter corresponds to the Atlantic coast [30] (950 km) (Figure 1A) and about $\frac{3}{4}$ of the population lives in coastal municipalities [31]. The Portuguese coast hosts several estuarine/lagoonal areas featuring salt marshes. Atlantic estuaries occur north of Mondego River (central Portugal), and Mediterranean estuaries occur on the south and west (southward of Mondego River) coasts of Portugal [32]. The salinity and biodiversity are higher in the latter than the former, particularly in the high marsh. Although both types are anthropically modified, the Mediterranean estuaries are the best-preserved [33].

Sado estuary, with an area of 23,560 ha [34], is a Mediterranean estuary located 40 km south of Lisbon at the mouth of a river with the same name (Figure 1B). Sado river's headwaters is located in "Serra da Vigia" (Ourique, Portugal) at 230 m of elevation [35]. Sado features the largest Portuguese watershed, with an area of circa 764,000 ha [36]. The climate (dry–subhumid [37] or subtropical [38]) can be described as uniform along the watershed, where the mean annual precipitation is 650 mm [35]. The river is classified as Mediterranean [39] and the flow ranges are between 1 m^3/s in the dry season and 80 m^3/s in the wet season [36]. The circulation and drainage within the estuary are essentially controlled by tides [40] because wind (which mainly blows from the north) only affects the surface water layer [35] and the river flow is too low. Ocean swell from the Atlantic Ocean cannot pass through the inlet, so the waves are usually smaller than 1 m inside the estuary.

Sado estuary is separated from the Atlantic Ocean by Tróia sandspit, a 25 km-long barrier trending NNW–SSE. Five growing phases were identified in Tróia sandspit, dated from 6500 years to present (Figure 1C) [41]. Two test areas featuring salt marshes were selected on the estuarine margin of this spit (Figure 1C–E) to apply the SMRM and the SLAMM. They are located in the NNW tip of Tróia sandspit, at Caldeira de Tróia (C. Tróia), which was further subdivided into two marsh expansions: north (C. Tróia (N)—Figure 1D) and south (C. Tróia (S)—Figure 1E) sectors. C. Tróia (S) was formed during the fourth growing phase of the sandspit (1870–1100 years before present), while C. Tróia (N) was installed during the most recent (fifth) growing phase (1100 years–present).

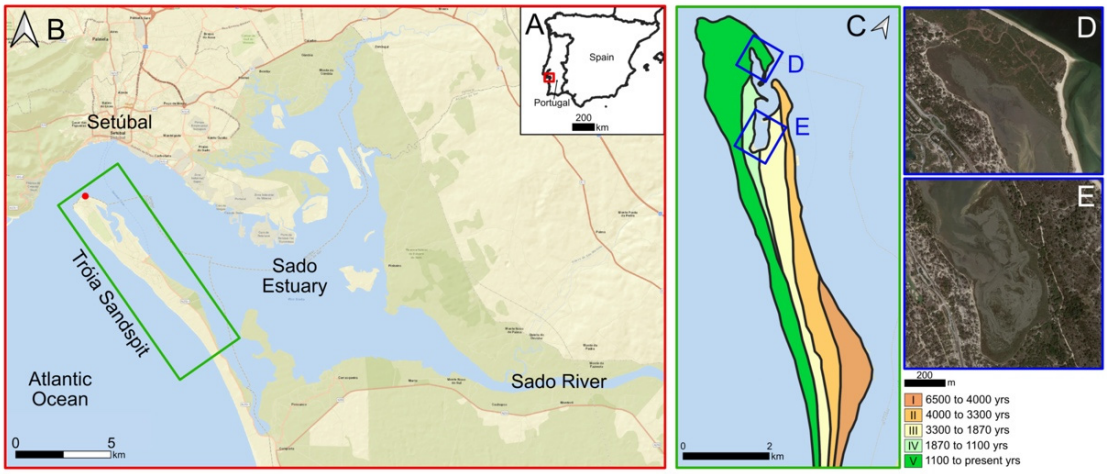

Figure 1. Test area locations. (**A**) Location in the Iberian Peninsula; (**B**) Sado estuary and Tróia sandspit. The red dot indicates the location of Setúbal-Tróia tide gauge; (**C**) Tróia sandspit evolution phases [41]; (**D**) C. Tróia (N) (Google satellite); (**E**) C. Tróia (S) (Google satellite).

C. Tróia (N) salt marsh extends over 4.3 ha and consists mainly of a high marsh, with small areas of a low marsh at lower heights. Adjacent to the salt marsh, there are two different environments: dunes of moderate slope (landwards) and tidal mudflats (seawards). C. Tróia (S) has similar characteristics to the northern sector, even though it displays a larger area (10.5 ha) and a larger proportion of low marsh vegetation.

3. Models

3.1. Simplified Marsh Response Model (SMRM)

The SMRM is a reduced complexity and two-dimensional rule-based model of marsh response to SLR that only requires the input of four parameters: (1) a high-resolution DTM, representing both the target marsh area and the adjacent surfaces (e.g., tidal flats, backbarrier flats, dunes, alluvial plains), with an acceptable spatial range, resolution, and quality to allow the simulation of marsh expansion; (2) critical tidal levels, representing a transition between main intertidal environments and vegetation sensitive to submersion time; in the test-cases addressed herein, the model considers mean high-water neap elevation (MHWN) as the critical boundary between the tidal flat and low marsh, mean high-water (MHW) as the transition between the low and high marsh, and mean high-water spring (MHWS) as the upper growth limit of the high marsh [42]; (3) at least one SLR projection, including an initial rate and an optional SLR acceleration value; (4) representative accretion/sedimentation rates for high marsh, low marsh, and tidal flat domains, which can remain invariant over time or change throughout the century (in this last case, acceleration values of accretion rates must be introduced). The SMRM works with several data sources, joining the results obtained from fieldwork and laboratory (accretion rates), monitoring equipment (tidal levels and SLR), physical models (SLR), and remote sensing (DTM).

The model was built considering the premises that present-day tidal amplitudes will not change significantly in future decades and that the salt marsh surface's signal and rate of evolution result from the balance between SLR rates and accretion rates (Table 1).

Table 1. Possible results for the evolution of salt marsh areas, considering the balance between SLR rates and accretion (Acc.) rates.

Situation	Possible Result
SLR rates < Acc. rates	Expansion
SLR rates ≈ Acc. rates	Stability
SLR rates > Acc. rates	Inundation

The process starts by comparing the elevation of each DTM cell with the elevation thresholds (as previously defined) at the reference time (2020). This step automatically classifies each cell as terrestrial environment, high marsh, low marsh, or tidal flat (subtidal areas are not discriminated). Next, the accretion rate characterizing each type of intertidal environment for each year is applied to the discretized surface and a new DTM is generated, corresponding to the next year's (2021) morphology. This process is repeated each year, and the transition levels are also adjusted yearly according to projected changes in sea level (Figure 2). The iteration sequence ends in the selected year as an output (2100 is the example shown herein, although decadal iterations were also performed).

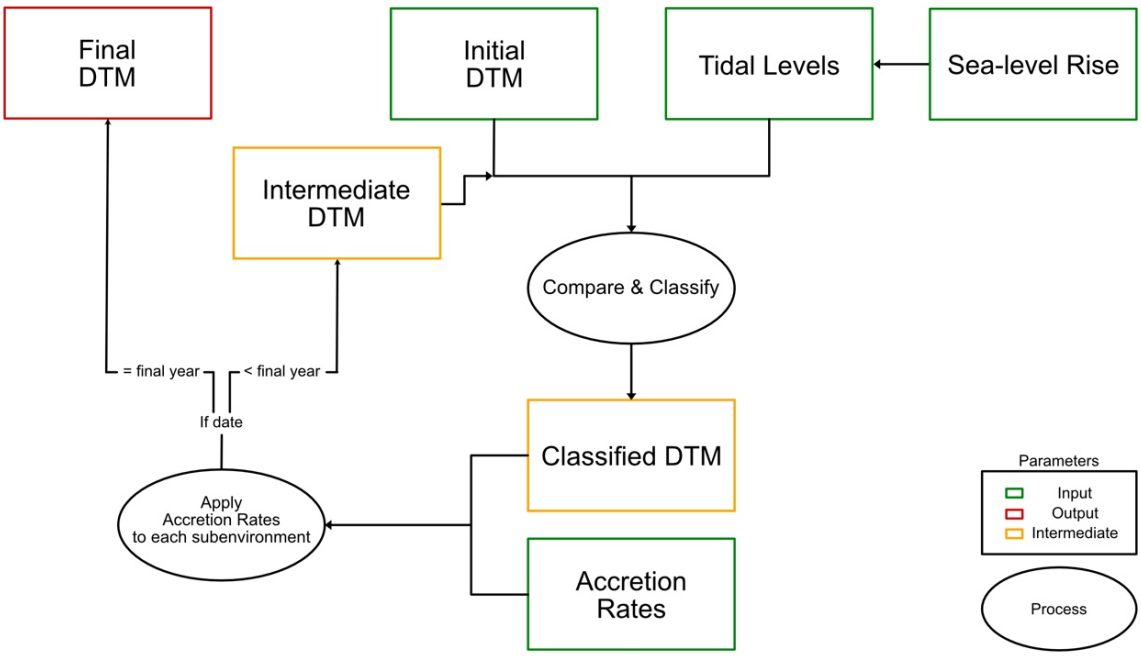

Figure 2. Flowchart showing relations among the parameters of SMRM, including inputs, outputs, intermediate parameters and processes.

The script to execute this set of steps was written in MATLAB R2018a (and updated to MATLAB R2020a) [43,44]. The output is a GeoTIFF file, which preserves the georeference of the original DTM. The final step is the generation of final maps and the determination of the new areas (high marsh, low marsh, and total area), based on tidal levels for the considered output year, which can be completed through any GIS software. In this work, this step was undertaken using ArcGIS Pro [45]. The SMRM script is available online [46].

In addition to the previous metrics, it is possible to obtain a parameter to estimate the maturity of the marsh, which depends on the ratio between high and low marsh areas and indicates the robustness of the salt marsh as a whole. In agreement with [42], a salt marsh is classified as young if the low marsh area is larger than the high marsh; intermediate, if both areas are broadly equivalent; and mature, if the high marsh is dominant over the low marsh area [42]. In order to obtain a quantitative indicator, an HM/LM (High Marsh/Low Marsh) ratio was established by the authors (HM/LM < 0.9 → young; HM/LM = [0.9–1.1] → intermediate; HM/LM > 1.1 → mature).

3.2. Sea Level Affecting Marsh Model (SLAMM)

The SLAMM model (version 6.7, Warren Pinnacle Consulting, Inc., Warren, VT, USA; Washington, DC, USA) [47,48] is also a two-dimensional rule-based model. It was initially developed to project the evolution of North American salt marsh areas until the end of the 21st century. However, SLAMM has not been widely applied to the Mediterranean–Atlantic salt marshes due to marked differences in vegetation, extent, and structure, although

its application seems acceptable [49]. SLAMM works in a complex relation among six processes: inundation, accretion, erosion, overwash, saturation, wind, and salinity.

In order to apply SLAMM to Portuguese test areas, spatial and site-specific parameters (which are detailed further below) are mandatory: digital terrain model (DTM), slopes, wetland category maps, tidal levels, diurnal tidal range, direction offshore, salt elevation, accretion rates, and at least one SLR scenario. To compare the obtained results with the results provided by SMRM, no more than the mandatory parameters were considered.

4. Parameters

The parameters considered to project the evolution of the test areas are local tidal levels, DTM, SLR, and accretion rates. Other parameters such as wind and waves are not used in SMRM and were not considered in SLAMM. Although sometimes these parameters seem relevant [50], they are not significant in the Sado estuary, as explained in Section 2 of this work. In addition, salinity can be considered uniform in a small area such as C. Tróia.

4.1. Local Tidal Levels

The first parameter considers the threshold limits to automatically classify each DTM cell as dune, high marsh, low marsh, and tidal flat. This work considers tidal levels because they correctly identify the transitions among the environments. However, other data can be considered for other areas, which can be chosen by the model's user.

Local tidal levels used in this study were modeled using harmonic analysis and based on data acquired by the Setúbal-Tróia tide gauge (years 1977, 1978, 1993, 1998, and 2005), located 2 km north of the study site (Figure 1B). Tide tables of 2000–2016 were computed from the harmonic model, mean values were evaluated, and a correction for the 2020 local mean sea level was applied (NMM1938, Cascais—the datum considered for all the heights presented in this study) [51,52].

SMRM and SLAMM use different tidal levels. SMRM considers the MHWN, MHW, and MHWS, whereas SLAMM uses heights of 30/60/90 days annual inundation periods. Furthermore, SLAMM also requires the introduction of the great diurnal tidal range (equivalent to the difference between mean highest high water and mean lowest low water levels) and the salt elevation (often defined as the elevation that is inundated by saltwater less than every 30 days in a year) [48]. These parameters were computed from the harmonic tidal model (Table 2).

Table 2. Tidal levels for SMRM and SLAMM in 2020.

SMRM			
MSL 0.19 m	MHWN 0.90 m	MHW 1.26 m	MHWS 1.61 m
SLAMM			
MSL 0.19 m	90 days 1.32 m	60 days 1.47 m	30 days 1.62 m
SLAMM site-specific parameters			
Great Diurnal Tidal Range 2.14 m		Salt Elevation 1.62 m	

4.2. Digital Terrain Model

The colonization of new marsh areas depends on the annual inundation periods, governed mainly by topography. The latter is a fundamental parameter since it influences many processes determining coastal change [53]. To evaluate the uncertainty of the inundation, it is essential to consider a remote sensing technique that accurately represents the studied area: a high-resolution DTM.

A DTM was obtained by interpolating a 2011 LiDAR survey performed by Agência Portuguesa do Ambiente (APA) and Direção Geral do Território (DGT), both Portuguese

public institutions. The horizontal resolution of the LiDAR varies between 1 and 2 m (2 m for intertidal environments such as salt marshes), and its vertical precision varies from 8 to 24 cm [30]. The LiDAR survey used topographic and bathymetric sensors, guaranteeing the data quality regardless of the surface type. Significant factors were also considered (topography and hydrography, temperature, humidity, precipitation, wind, water turbidity, pollution, flora, and fauna) to produce the final DTM [30].

The studied salt marshes display many tidal channels less than 2 m wide, matching the horizontal resolution of the considered DTM. Consequently, some of these channels are not well represented and generate sinks. Considering that tidal channels were not separately represented in simulations produced by both models, these artifacts (sinks) were leveled with the surrounding surface elements using the fill tool provided by ArcGIS Pro.

Heights of homologous points measured in the field using a DGPS-RTK (Leica Viva NetRover GS08) and yielded by the DTM were compared to validate the accuracy of the terrain model. In total, 2722 points distributed over the high marsh, low marsh, and tidal flat of both C. Tróia (N) (1844 points) and C. Tróia (S) (878 points) were measured (Figure 3, Table A1) between 2016 and 2021. Although there is a gap of at least five years between the LiDAR survey and DGPS records, the difference should only correspond to the sedimentation that occurred in this period, because the erosion of marshes is not laminar and usually occurs at the edges [54].

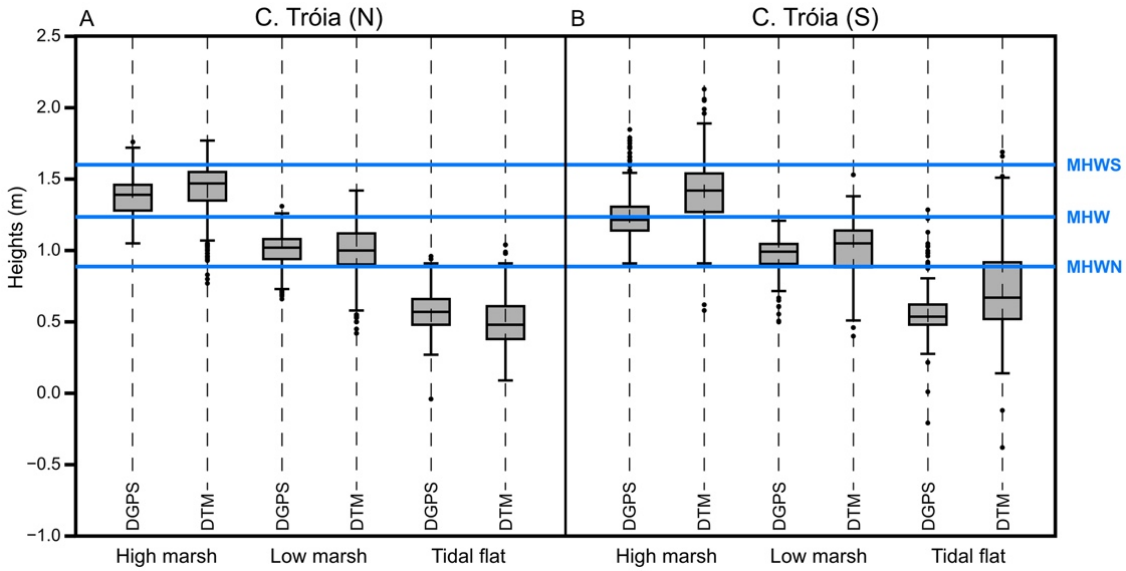

Figure 3. Boxplots showing the distribution of heights obtained through DGPS and DTM. (**A**) C. Tróia (N); (**B**) C. Tróia (S). Blue lines indicate the heights of local critical tidal levels: MHWS—mean high water spring; MHW—mean high water; MHWN—mean high water neap.

In general, each environment is distributed between the theoretical tidal limits, so the SMRM will correctly classify each pixel of the DTM. On average, heights extracted from the DTM are higher than those obtained in the field, which can be justified by the salt marsh vegetation or water, even though these parameters were considered during the survey and data processing. C. Tróia (N) high marsh is higher than the high marsh in the southern sector. Although there are natural differences between the two data sources, the DTM is considered a reasonable morphologic representation of the study areas.

Besides the DTM, SLAMM requires a slope file and a *.txt file with each pixel's SLAMM wetland categories. The slope file was obtained from the original DTM, and the categorization was completed manually according to the classification provided by this model's Technical Documentation [47]. SLAMM does not clearly differentiate high and low marsh. Instead, it considers "regularly flooded marsh" and "irregularly flooded marsh", which was associated with low and high marsh, respectively, in agreement with other

authors [49]. Dunes were classified as undeveloped dry land since they are vulnerable to inundation and colonization by marsh vegetation.

A statistical evaluation of the DTM accuracy was performed in addition to the comparison between the DGPS and DTM data. The root mean square error (RMSE) was determined, considering both data sources (Equation (1), Table 3). The RMSE is a metric widely used to express the vertical accuracy of elevation datasets [55].

$$RMSE = \sqrt{\frac{\sum(Z_{DTM\ i} - Z_{DGPS\ i})^2}{n}} \quad (1)$$

Table 3. RMSE and L.E. of C. Tróia (N) and (S) salt marshes DTM.

			C. Tróia (N)		
	Global	Dune	High marsh	Low marsh	Tidal flat
RMSE	17 cm	29 cm	13 cm	18 cm	14 cm
L.E.	33 cm	57 cm	25 cm	36 cm	27 cm
			C. Tróia (S)		
	Global	Dune	High marsh	Low marsh	Tidal flat
RMSE	22 cm	39 cm	21 cm	15 cm	31 cm
L.E.	43 cm	76 cm	41 cm	29 cm	60 cm

Z_{DTM} is the height of each point in the DTM, Z_{DGPS} is the height of each homologous point measured with the DGPS, n is the number of points being checked, and i is an integer from 1 to n. Besides the RMSE, the linear error (L.E.) was also determined at a confidence level of 95% (the metric used by the National Standard for Spatial Data Accuracy (Federal Geographic Data Committee, 1998)) (Equation (2), Table 3).

$$L.E._{(95\%)} = 1.96 \times RMSE \quad (2)$$

A global RMSE of 17 cm for C. Tróia (N) was obtained, which is compatible with the vertical accuracy of the DTM. The error is higher on dunes, probably because the DGPS data were measured between 2016 and 2021 and the DTM corresponds to a survey of 2011. The RMSE of the C. Tróia (S) salt marsh is globally higher. However, the global value is within the accuracy limits of the DTM. An RMSE of 17 cm was considered in the sensitivity analysis of the model performed in C. Tróia (N).

In this study, the DTM is considered static until the end of the century due to negligible vertical land motion (either isostatic or tectonic driven) compared with the magnitude of sea level changes. However, changes can occur due to land motion, and if that is the case, they can be added to the DTM error or to SLR.

A combination of data on absolute mean sea level derived from satellite observations with high-precision GPS data of vertical ground motion measured near tide gauges and relative mean sea level data measured at those tide gauges may be used to decouple eustatic from vertical land movements at shorter timescales and evaluate uncertainty. The magnitude of vertical land movement in the Cascais region (some 50 km north of Sado estuary) has been assessed by [52], comparing the 1990–2019 relative sea level data, retrieved from Cascais tide gauge, with 1993–2016 data on absolute sea level derived from satellite altimetry. He inferred vertical uplift rates from 0.08 to 0.28 mm/year. Different results have been obtained by [56]. These authors computed vertical land motions along the Iberian Atlantic coast using GPS time series with more than 8 years of observations. GPS-derived estimates of the vertical land movement were further used to correct data on sea level obtained at tide gauges. The latter was compared with satellite altimetry absolute sea level. In Cascais region, tide gauge results suggest small subsidence (-0.40 ± 0.08 mm/year) over 1997–2020. Another recent study [57] analyzed a global database of high-precision GPS data acquired after 2002 to set up an interpolated field of vertical land movement rates, from

which median rates at the location of tide gauges in the Permanent Service for Global Mean Sea Level may be obtained ([57] provides methodological details). Vertical land movements shown in this study for Cascais and Setúbal-Tróia tide gauges indicate low subsidence at both stations, at rates of -0.766 ± 0.238 and -0.766 ± 0.320 mm/year, respectively. As correctly pointed out by [56,57], the above estimates should be taken with caution, given that different studies use different methodological approaches, contrasting lengths of the data series, heterogeneity in the spatial distribution of GPS source stations, and possible undocumented problems affecting both GPS and tide-gauge stations, and differences in data analysis and correction.

The contrast between the magnitude of vertical land motion (in the order of 10^{-1} mm/year) affecting the study area recently and coeval multi-decadal changes in relative sea level (in the order of 10^{0} mm/year) indicates that eustatic components have largely dominated the latter. The future increase in sea level rise rate (in the order of 10^{1} mm/year by the end of the 21st century) will enhance this contrast. It is reasonable to disregard the influence of vertical land motions in relative sea-level patterns, and marsh inundation projected until the end of the 21st century for Sado salt marshes, considering the objectives and timescale of this study.

4.3. Sea-Level Rise Scenarios

This study considers four SLR scenarios: IPCC RCP4.5 and RCP8.5 [58], Mod.FC_2b [52], and NOAA Extreme [59]. IPCC SLR scenarios were chosen to consider global projections, MOD.FC_2b is an empirical projection based on the Cascais (Portugal) tide gauge, and NOAA Extreme is a high-end SLR projection, which can be useful for land management measures.

SMRM requires an initial SLR rate and an acceleration value. These parameters are published for MOD.FC_2b, but only decadal absolute mean sea-level values are available for IPCC RCP4.5/RCP8.5 and NOAA Extreme. The provided values were plotted, and a polynomial function was calculated. The initial SLR rate (2020) and the acceleration were obtained through the first and second derivates of the functions, respectively (Table A2). All the SLR projections were adjusted to the Portuguese datum to be concordant with other parameters (Figure 4). A remark must be made on the NOAA Extreme projection since the 2020 SLR rate inferred from the respective model gives a much higher rate than the most recent observed SLR rate [52]. In 2100, such SLR would be only possible through an exponential model, related to a disruptive process, that could respect the actual SLR rates and the final sea level. However, the model and respective values of SLR and rates were used as presented by the report's authors [59].

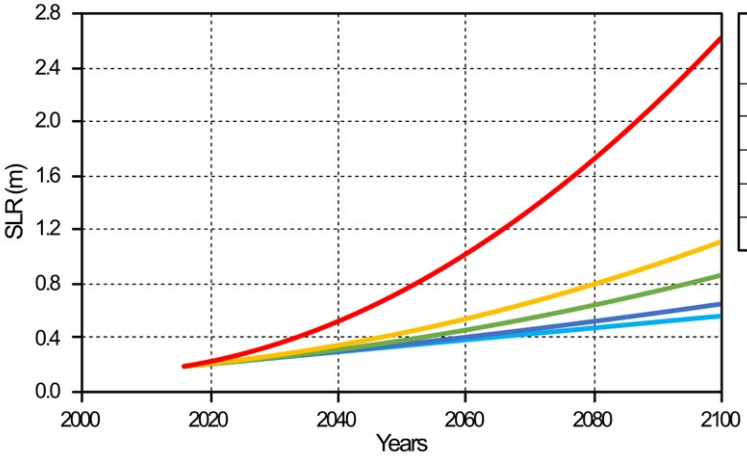

SLR Scenario	Rate 2020 mm/year	Acceleration mm/year²
IPCC RCP2.6	4.463	0.000
IPCC RCP4.5	4.449	0.030
IPCC RCP8.5	4.340	0.097
MOD.FC_2b	5.260	0.152
NOAA Extreme	9.506	0.505

Figure 4. SLR evolution until 2100. SLR rates and acceleration, regarding the Portuguese local datum, for the considered scenarios: IPCC RCP2.6/4.5/8.5, MOD.FC_2b, and NOAA Extreme.

In addition to the previous scenarios, the IPCC RCP2.6 SLR projection was also included to perform a sensitivity analysis, since it can be described as a scenario with an almost linear behavior.

Many different scenarios can be incorporated in models of marsh response to SLR. It is fundamental to select a wide range of scenarios, to obtain different results. The previously presented scenarios include rises in sea level from 55 (IPCC RCP2.6) to 261 cm (NOAA Extreme) until 2100, and intermediate values (111 cm—MOD.FC_2b). Other SLR scenarios, e.g., [60], are within the presented set of values.

SLAMM allows the user to introduce a specific SLR projection or to select an SLR scenario from a list (mainly from IPCC). However, the included SLR projections are from the outdated IPCC 4th Assessment Report [61].

4.4. Accretion Rates

Sediment availability is fundamental for the survival of saltmarsh areas [62]; thus, any models trying to predict how these areas will evolve need to include this parameter. In this paper, sedimentation and accretion are used interchangeably to mean "the vertical increase in surface elevation (in mm) relative to a specific layer of soil" [63].

Vertical accretion combines the deposition and erosion of sediments, the accumulation of dead biomass on the marsh surface, and a certain amount of local subsidence (also called settlement or autocompaction) [63]. Many factors can influence the vertical accretion rate (e.g., sediment availability, presence of vegetation, tidal dynamics). The advantage of using radiochronology (e.g., ^{137}Cs and ^{210}Pb dating) to derive sedimentation rates is that the results already incorporate most of these factors [63].

In C. Tróia (N), accretion rates derived from the ^{210}Pb dating method are 2.9 mm/year in the high marsh, 3.0 mm/year in the low marsh, and 2.5 mm/year in the tidal flat. From the ^{137}Cs measurements and considering 1963 maximum atmospheric fallouts as the time marker, the sedimentation rates are 2.9, 2.9, and 3.3 mm/year, respectively. Appendix B presents the results from the ^{137}Cs and ^{210}Pb determination, and a detailed explanation of the used methods. The obtained values represent the last century's sedimentation pattern and are suitable for integrating a model that will not exceed 2100 in its projections. We assume that accretion rates will not vary until the end of the century. Regarding the proximity of the two study sites and their similarities, the same accretion rates were also assumed for C. Tróia (S) marsh. Furthermore, other studies performed nearby found values of sedimentation rates ranging from 2.80 to 4.40 mm/year (depending on the technique) in the marshes of Malha da Costa (38°25′58″N, 8°49′31″W) and Faralhão (38°31′04″N, 8°47′03″W), both on the Sado estuary [64]. The similarity of the results demonstrates how consistent sedimentation is in this region, implying that, in the absence of new measurements, the obtained accretion rates in one marsh can be applied when modeling others located nearby.

Both SMRM and SLAMM consider one accretion rate for each environment, which is a simplification, since there are many aspects not considered: accretion rates will usually decrease with the increase in height, accretion rates tend to be higher near the tidal creeks, and others. Furthermore, changes in SLR could potentially affect sediment availability in the entire estuary. Investigating this aspect is, in itself, an entirely separate work. It might be possible to identify different accretion rates in areas with very high sedimentation rates over time. SMRM considers the possibility of working under nonlinear accretion rates. This is done by introducing a positive or negative acceleration value that affects the initial rates.

5. Application of SMRM to the Test Areas and Comparison with SLAMM

This section presents the results of SMRM application to both sectors of C. Tróia (the output datasets are available in [65]). They are similar in the two test areas, although the southern sector is less resilient to SLR. In addition, the obtained results are compared with SLAMM simulations for C. Tróia (N). The comparison is presented according to each SLR

scenario's severity (IPCC RCP4.5/8.5, MOD.FC_2b, and NOAA Extreme). In line with each SLR projection, the obtained results are quite different (Table 4).

Table 4. Area and HM/LM ratio values for 2020, 2050, and 2100 for C. Tróia (N) and C. Tróia (S) salt marshes, considering IPCC RCP4.5/RCP8.5, MOD.FC_2b, and NOAA Extreme SLR scenarios using SMRM and SLAMM.

	Scenario	SMRM						SLAMM					
		2020		2050		2100		2020		2050		2100	
		Area (ha)	HM/LM	Area (ha)	HM/LM	Area (ha)	HM/LM	Area (ha)	HM/LM	Area (ha)	HM/LM	Area (ha)	HM/LM
C. Tróia (N)	IPCC RCP4.5	4.48	2.9	4.49	2.3	4.33	1.0	4.31	2.8	4.30	2.2	3.99	0.8
	IPCC RCP8.5			4.45	2.1	3.79	0.4			4.27	2.0	3.63	0.3
	MOD.FC_2b			4.36	1.4	1.89	0.7			4.17	1.3	1.67	0.5
	NOAA Extreme			3.42	0.3	1.25	1.2			3.25	0.2	1.03	0.8
C. Tróia (S)	IPCC RCP4.5	10.29	1.4	10.12	1.2	9.10	0.8	10.31	1.4	9.93	1.2	8.60	0.7
	IPCC RCP8.5			9.95	1.2	6.65	0.4			9.74	1.1	6.37	0.4
	MOD.FC_2b			9.44	1.0	4.39	1.1			9.22	0.9	4.01	0.8
	NOAA Extreme			5.98	0.3	5.40	1.5			5.71	0.3	3.81	1.0

The results are very similar for both models. However, some differences should be noted. The initial area is manually defined based on field and satellite imagery observation. Nevertheless, each model adjusts the initial area according to the local tidal levels (SMRM) or other relevant parameters (slope, salt elevation, great diurnal tidal range—SLAMM). For this reason, in 2020, the area is not precisely the same for both models. Thus, in the C. Tróia (N) salt marsh, the initial area is overestimated by 3% with SMRM and 1% with SLAMM (Figure 5A,B). In the case of C. Tróia (S), the real limits coincide with the local tidal levels (Figure 5C,D).

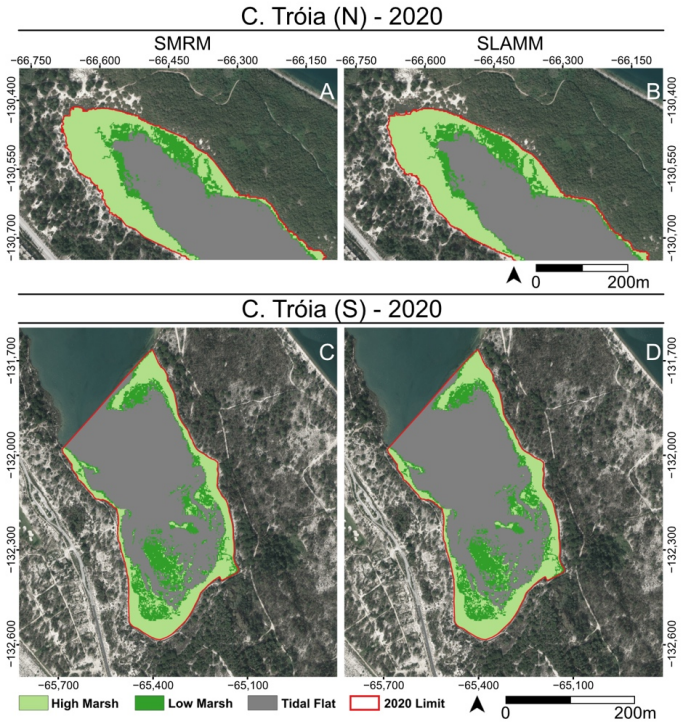

Figure 5. Modeled morphological map for 2020 for C. Tróia (N) and (S), using SMRM (**A**,**C**) and SLAMM (**B**,**D**). Coordinate system: ETRS1989 (PT06). Basemap: 2014–2015 DGT Orthophotos.

Considering IPCC RCP4.5 (SLR of 65 cm until 2100), SMRM projects that C. Tróia (N) will maintain its area until 2050 and a loss of only 3% is expected until 2100 (4.33 ha) (Figure 6A). The HM/LM ratio will decrease to 2.3 and to 1.0 by 2050 and 2100, respectively, which is clear in the morphological maps (Figure 7A,C). C. Tróia (S) will lose 2% (10.12 ha) and 12% (9.10 ha) of its area (Figure 8A) and the HM/LM ratio will be 1.2 and 0.8 in 2050 and 2100 (Figure 9A,C). The losses are greater with SLAMM: in C. Tróia (N), there will be no losses in the area until 2050 and a loss of 7% (Figure 6B) (HM/LM = 2.2/0.8 for 2050/2100—Figure 7B,D) is expected until 2100. In C. Tróia (S), the area will be reduced by 4% and 17% until 2050 and 2100 (Figure 8B) (HM/LM = 1.2/0.7 for 2050/2100—Figure 9B,D).

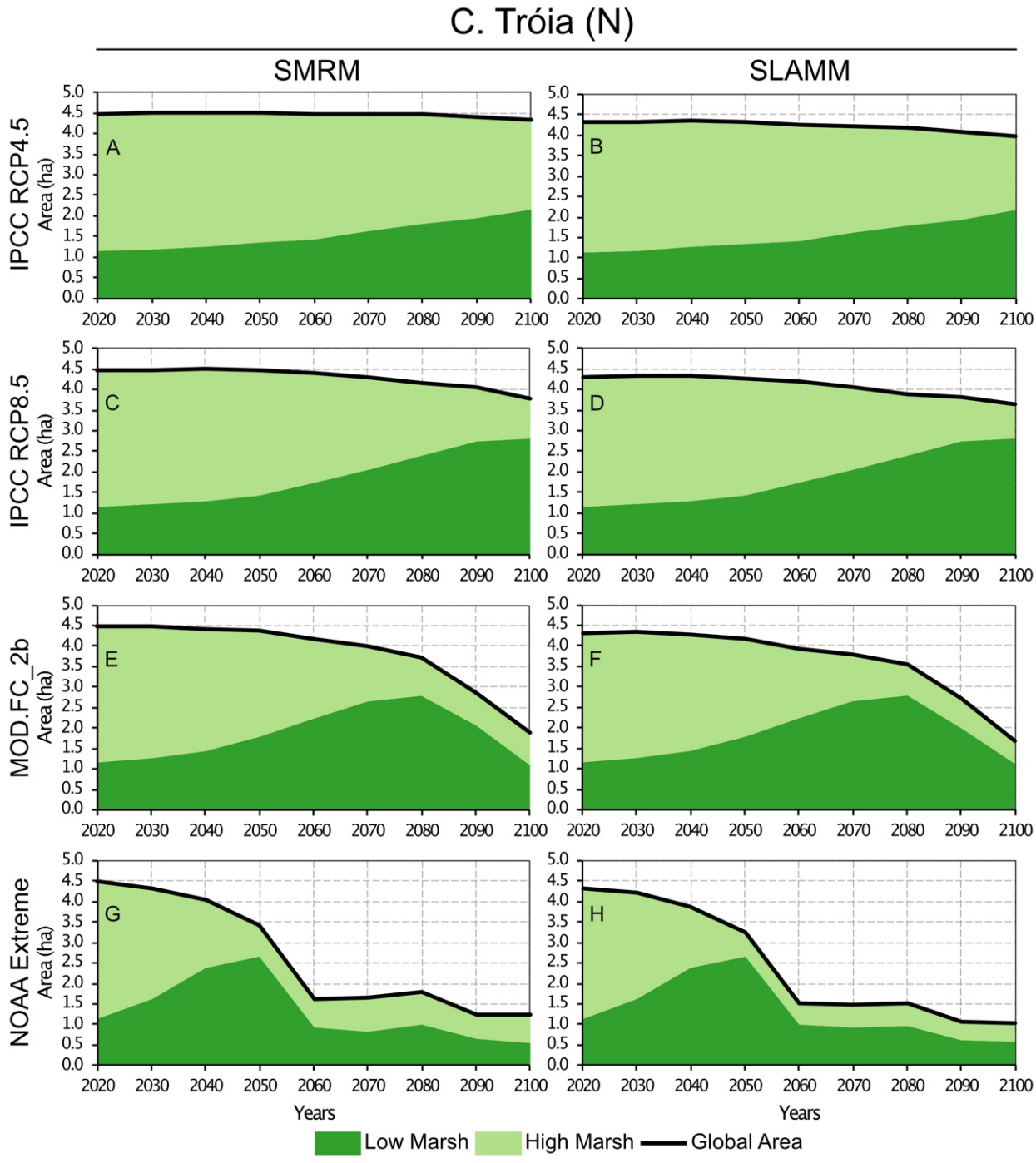

Figure 6. C. Tróia (N) decadal area evolution until 2100, using SMRM and SLAMM, respectively, considering IPCC RCP4.5 (**A**,**B**), IPCC RCP8.5 (**C**,**D**), MOD.FC_2b (**E**,**F**), and NOAA Extreme (**G**,**H**).

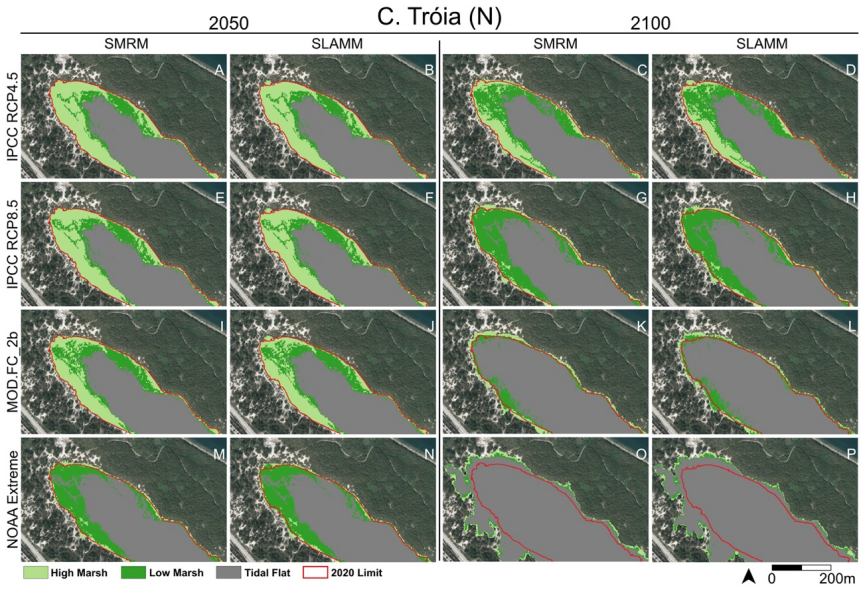

Figure 7. C. Tróia (N) salt marsh morphological maps for 2050 and 2100, using SMRM and SLAMM. Results are presented for the considered SLR scenarios: IPCC RCP4.5 (**A**–**D**), IPCC RCP8.5 (**E**–**H**), MOD.FC_2b (**I**–**L**), and NOAA Extreme (**M**–**P**).

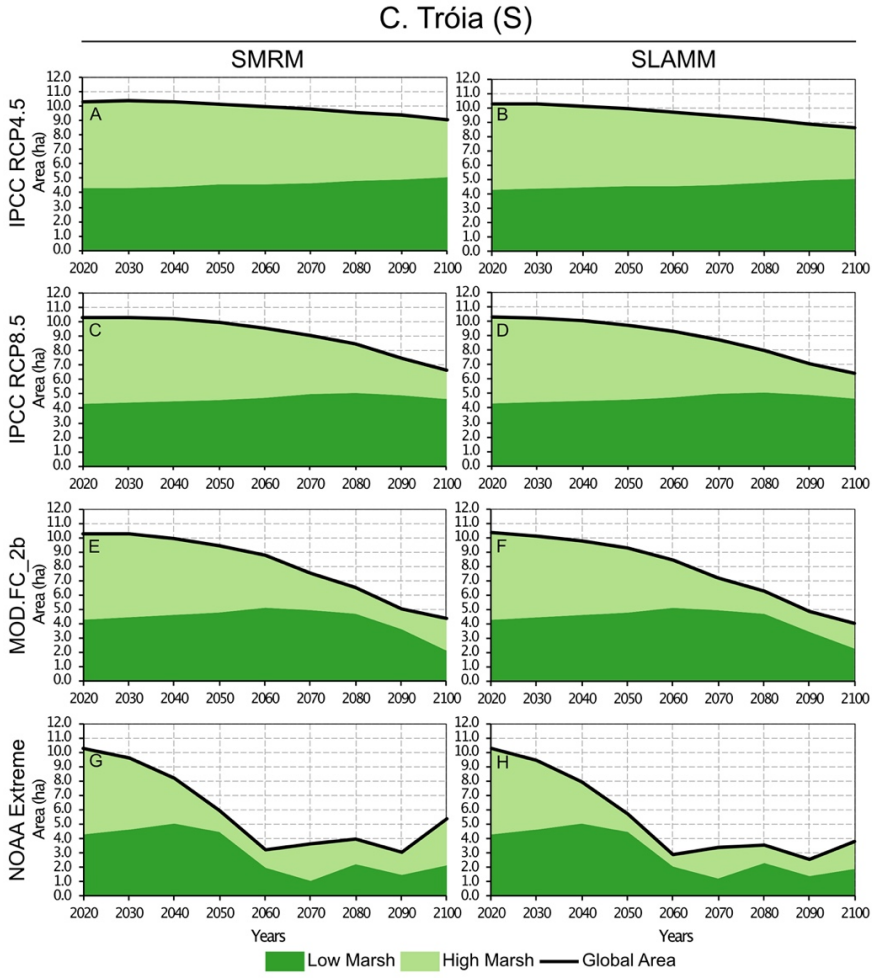

Figure 8. C. Tróia (S) decadal area evolution until 2100, using SMRM and SLAMM, respectively, considering IPCC RCP4.5 (**A**,**B**), IPCC RCP8.5 (**C**,**D**), MOD.FC_2b (**E**,**F**), and NOAA Extreme (**G**,**H**).

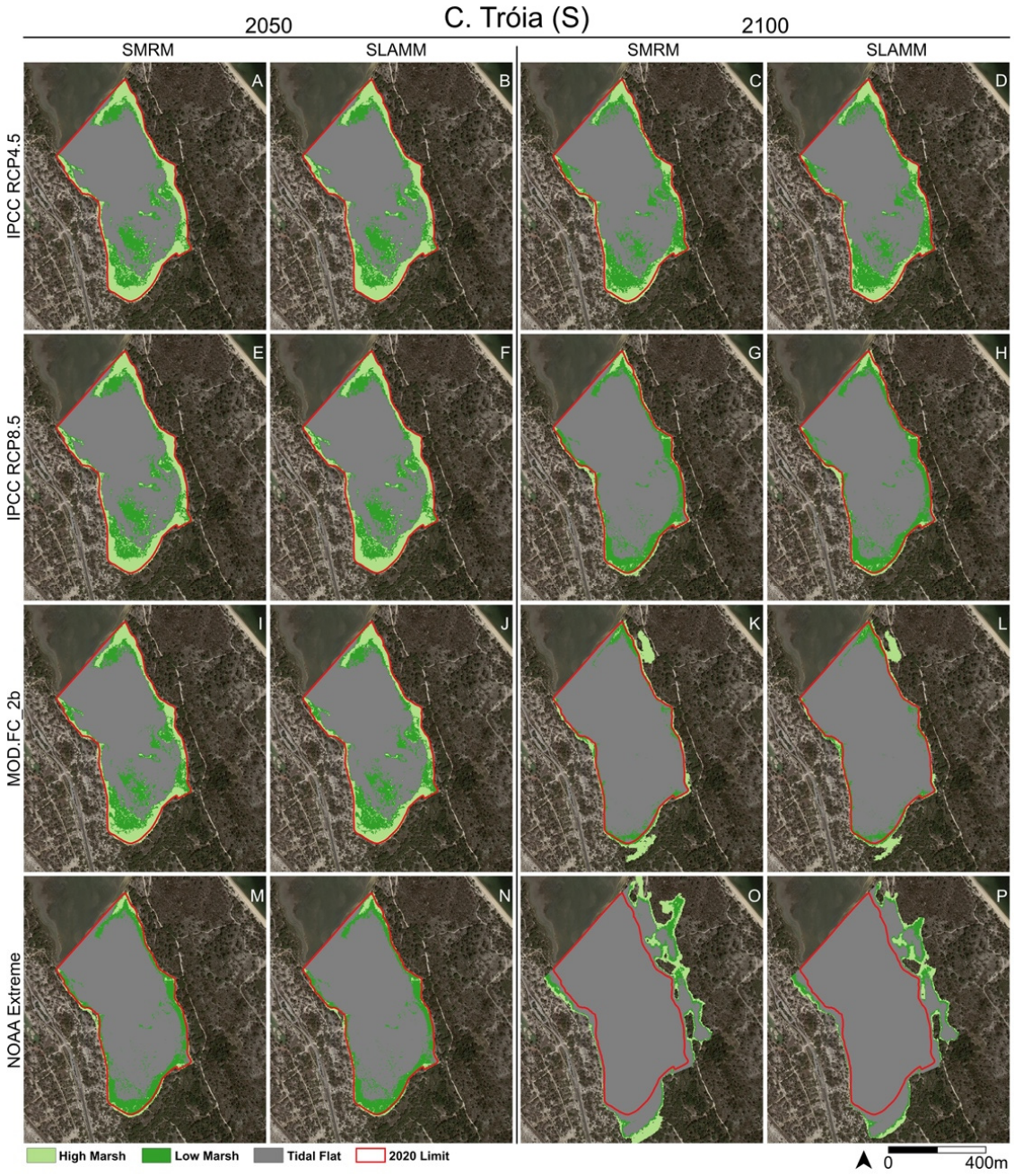

Figure 9. C. Tróia (S) salt marsh morphological maps for 2050 and 2100, using SMRM and SLAMM. Results are presented for the considered SLR scenarios: IPCC RCP4.5 (**A**–**D**), IPCC RCP8.5 (**E**–**H**), MOD.FC_2b (**I**–**L**), and NOAA Extreme (**M**–**P**).

With IPCC RCP8.5 (SLR of 86 cm until 2011), SMRM projects 1% (4.45 ha) and 15% (3.79 ha) losses until 2050 and 2100 for C. Tróia (N) (Figure 6C). The HM/LM ratio will decrease to 2.1 and 0.4 for these reference dates, respectively (Figure 7E,G). In C. Tróia (S), the area will be reduced by 3 and 35% (Figure 8C) and the HM/LM ratio will be 1.2 and 0.4 in 2050 and 2100 (Figure 9E,G). With SLAMM, C. Tróia (N) area will decrease by 1% and 16% (Figure 6D) (HM/LM = 2.0/0.3 for 2050/2100—Figure 7F,H) and C. Tróia (S) will decrease by 6% and 38% until 2050 and 2100 (Figure 8D), respectively (HM/LM = 1.1/0.4 for 2050/2100—Figure 9F,H).

The SMRM with the MOD.FC_2b SLR scenario (111 cm until 2100) produces major changes until the end of the century. In C. Tróia (N), the area will be reduced by 3% (4.36 ha)

and 58% (1.89 ha) (Figure 6E) and the HM/LM ratio will be 1.4 and 0.7 until 2050 and 2100 (Figure 7I,K). For C. Tróia (S), the losses will be almost identical: the area will be reduced by 8% (9.44 ha) and 57% (4.39 ha) in 2050 and 2100 (Figure 8E). However, the HM/LM ratio will be 1.0 and 1.1, respectively (Figure 9I,K). SLAMM produces area losses of 3% and 61% for C. Tróia (N) (Figure 6F) (HM/LM = 1.3/0.5 for 2050/2100—Figure 7J,L) and of 11% and 61% for C. Tróia (S) for the reference dates (Figure 8F) (HM/LM = 0.9/0.8 for 2050/2100—Figure 9J,L).

Finally, considering SMRM with NOAA Extreme (261 cm of SLR until 2100), the area will be reduced by 24% (3.42 ha) and 72% (1.24 ha) in 2050 and 2100 in C. Tróia (N) (Figure 6G). The HM/LM will be 0.3 and 1.2, showing a recovery by the end of the century (Figure 7M,O). In C. Tróia (S), the losses in the area will be almost the same in 2050 and 2100: 42% (5.98 ha) and 48% (5.40 ha) (Figure 8G). The HM/LM ratio decreases to 0.3 in 2050 and increases to 1.5 in 2100 (Figure 9M,O). SLAMM produces area losses of 25% and 76% in C. Tróia (N) (Figure 6H) (HM/LM = 0.2/0.8 for 2050/2100—Figure 7N,P) and 45% and 63% in C. Tróia (S) until 2050 and 2100 (Figure 8H) (HM/LM = 0.3/1.0 for 2050/2100—Figure 9N,P).

In general terms, the results obtained with the two considered models are similar for both study areas.

6. Sensitivity Analysis

6.1. Methodology

A sensitivity analysis was performed on the C. Tróia (N) salt marsh to evaluate the influence of each parameter on the result of SMRM, establishing three risk levels: low, medium, and high (Table 5). For each level, each parameter (DTM, SLR, and accretion rates) was combined in all the available possibilities. In total, 36 different combinations were considered in this exercise and the results were plotted in boxplots (Figure 10).

Table 5. Risk levels for the sensitivity analysis performed with SMRM to the C. Tróia (N) marsh.

Risk	DTM	SLR	Acc. Rates
Low	SLR − RMSE	IPCC RCP2.6 IPCC RCP4.5	5.46/5.84 mm/year (tidal flat/marsh)
Medium	-	MOD.FC_2b	2.73/2.92 mm/year (tidal flat/marsh)
High	SLR + RMSE	NOAA Extreme	0 mm/year

Each risk level includes different values for each evaluated parameter (DTM, SLR, and Accretion Rates). The three risk levels of the DTM were formed through the inundation heights, adding or subtracting the RMSE to the SLR [53]. Four SLR scenarios were considered: the conservative one (low risk—IPCC RCP4.6), the intermediate (medium risk—MOD.FC_2b), and the high-end (high risk—NOAA Extreme). In addition, IPCC RCP2.6 was also considered since it is a scenario with an almost linear behavior. Lastly, the determined accretion rates were used for the medium-risk scenario. For the low risk, accretion rates were doubled (5.8 mm/year for high and low marsh; 5.5 mm/year for tidal flat) and eliminated (0 mm/year) for the high-risk scenario. The evaluated results were the change in the global area as well as the inundation area (which is the new area colonized by marsh that is currently terrestrial area) until 2100.

Results yielded by SMRM are contained in a GeoTIFF file. Therefore, it is possible to determine the total addressed area, partial high and low marsh areas in the simulated time horizon, and the inundation area (which is the area now colonized by marsh vegetation). Therefore, both the changes in total and inundation areas in 2100 were used in the sensitivity analysis.

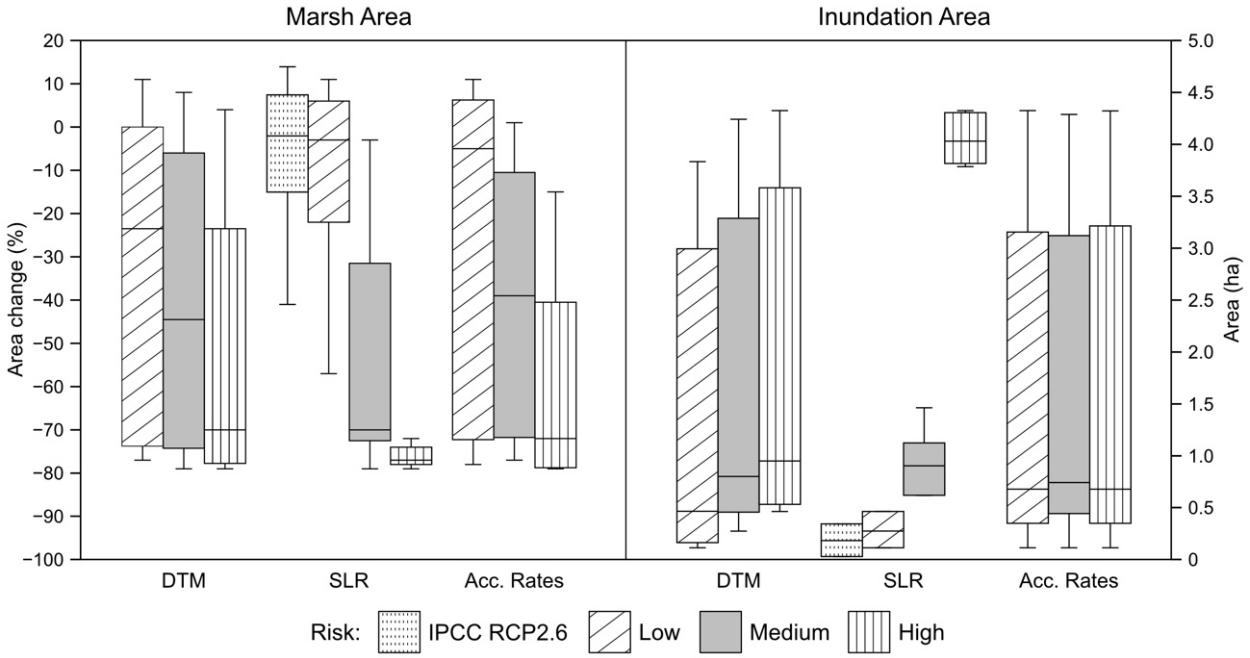

Figure 10. Boxplots of the sensitivity analysis performed on SMRM. The analysis includes three levels of risk for each evaluated parameter (DTM, SLR, and accretion rates—Acc. Rates). The analyzed results are the marsh area and the inundation area in 2100.

6.2. Results

The sensitivity analysis results show that SLR is the most critical parameter to consider in the evolution of the marsh areas, because each SLR scenario produces a different set of results. For instance, when the NOAA Extreme scenario is considered, C. Tróia (N) marsh will lose between 70% and 80% of its original area until the end of the 21st century, no matter which risk level is selected for the remaining parameters. An exception is made for IPCC RCP2.6 and RCP4.5, which may produce similar results. Accretion rates are also a fundamental input for the model (as other authors have reported [66,67]). Double rates (low risk) may produce lower variations in the global area than the medium risk level. However, the most significant impacts are observed when no accretion rates are considered (high risk). Thus, it is possible to infer that accretion rates are an essential parameter to consider, even if an increase in the value does not produce proportionally different results. The RMSE of the DTM seems to have an impact on the global area that is proportional to the size of the error.

Regarding the inundation area, SLR is also the most relevant parameter, although only NOAA Extreme (high risk) produces a very significant change in the result. As in the global area evolution, the RMSE of the DTM also impacts the inundation area proportionally to the error's size. Lastly, accretion rates do not influence the inundation area, which is only controlled by the inundation height, which is different according to the chosen SLR scenario and RMSE of the DTM.

7. Discussion

The discussion of this work is based on three topics: the advantages and drawbacks of applying SMRM to marsh areas; the projection of the evolution of the test areas; and the possibility of extrapolating the results to other areas.

Using a reduced-complexity model allows for obtaining projections of marsh evolution considering only the fundamental data. This case includes tidal levels, SLR, accretion rates, and the local morphology. Using as few parameters as possible without compromising the reliability of the results is essential to study many areas where there are not sufficient available data or to perform quick preliminary projections. Furthermore, these advantages

are crucial to undertake the correct land management of these areas (e.g., to define which areas should remain free of occupation).

In order to evaluate the reliability of the produced results, a comparison with SLAMM was performed. Besides the SMRM inputs, SLAMM also requires at least the following additional parameters: slopes, wetland categories map (spatial parameters), great diurnal tidal range, and salt elevation (site-specific parameters). SLAMM also allows the user to choose among predefined SLR scenarios, which are outdated. The alternative is to input the mean sea-level position for each year until the end of the century. The results obtained with SMRM are quite similar to those obtained with SLAMM regarding the global area, HM/LM, and marsh distribution. For the initial year, both models recalculate the marsh area, which is the basis for the simulations performed until the end of the century. SLAMM seems more accurate in representing the initial salt marsh area, although the differences are not significant. Differences between models are always related to the maximum inundation line—the behavior of seaward limits is always similar in both models.

The sensitivity analysis shows that the parameter that most significantly controls the evolution of marsh areas with SMRM is the SLR—the result is clearly different according to the chosen scenario. It is the most powerful parameter regarding both the evolution of the marsh area and the inundation area. Conservative and intermediate scenarios produce comparable results, but the high-end scenario can project an almost complete inundation of these areas. The other two parameters are relevant in different ways. When the RMSE of the DTM is considered, a proportional change in the evolution of the marsh is identified (i.e., the greater the error, the larger the expected inundation, e.g., [53,68,69]). Accretion rates are crucial for estimating the marsh area in the future, but they are not relevant to determining the inundation area, since it only depends on the DTM and SLR. On the one hand, if the accretion rates double, it seems that the results are hardly affected. On the other hand, considering no accretion rates, a major difference in the results can be produced.

Many studies have been published regarding the evolution of wetlands, trying to find a global tendency of evolution, even if each wetland can have its behavior in the future [31]. Recently, marsh areas have kept pace with SLR [70], with small area losses [71]. However, there are different results (from different studies) on the future of salt marshes. Some authors project that in the future, these areas will survive with conservative SLR scenarios [72] or even if high-end scenarios are considered [73], but other studies always project a significant loss in area in these environments [74]. The results of SMRM indicate that the accommodation space landwards will be fundamental to the survival of wetlands, as other authors previously suggested [75]. Even so, it is reasonable to assume that the stability of marsh areas should be guaranteed in the first half of the century, mainly when conservative or intermediate SLR scenarios are considered. However, the HM/LM ratio reduction seems inevitable in all projections for both study areas, mainly in the second half of the century. This reduction occurs because, when sea level rises, the tidal limits that define each environment's existence also increase in height. If accretion rates are not high enough to compensate for the SLR rates, areas currently colonized by high-salt marsh vegetation will suffer longer periods of annual flooding. Consequently, these areas will be colonized by vegetation more tolerant to inundation than high marsh vegetation. If sea level continues to rise, the annual inundation periods in these areas will also continue to increase. They may reach values that will be no longer compatible with low marsh vegetation. As a result, these areas will not keep any vegetation type, and will become non-vegetated areas (tidal flats). The consequences of these losses are reflected in the diminishing of the ecosystem's services, such as physical protection or carbon sequestration [76]. In fact, the loss of marsh areas due to SLR could imply an emission of CO_2 to the atmosphere equivalent to the increase in global greenhouse emissions [77]. That is why the preservation of marshes is seen as a natural climate solution to climate changes [78,79].

In this work, four theoretical phases in the evolution of salt marsh areas until the end of the 21st century were identified (Figure 11): (I) stability, (II) significant loss of maturity, (III) significant loss of area and, in cases, (IV) a partial area recovery. High-end SLR scenarios

tend to generate more evolution phases than conservative projections (this is always visible in Figures 7 and 8). The behavior is similar in all cases, which is different in the timing of each evolution phase occurrence.

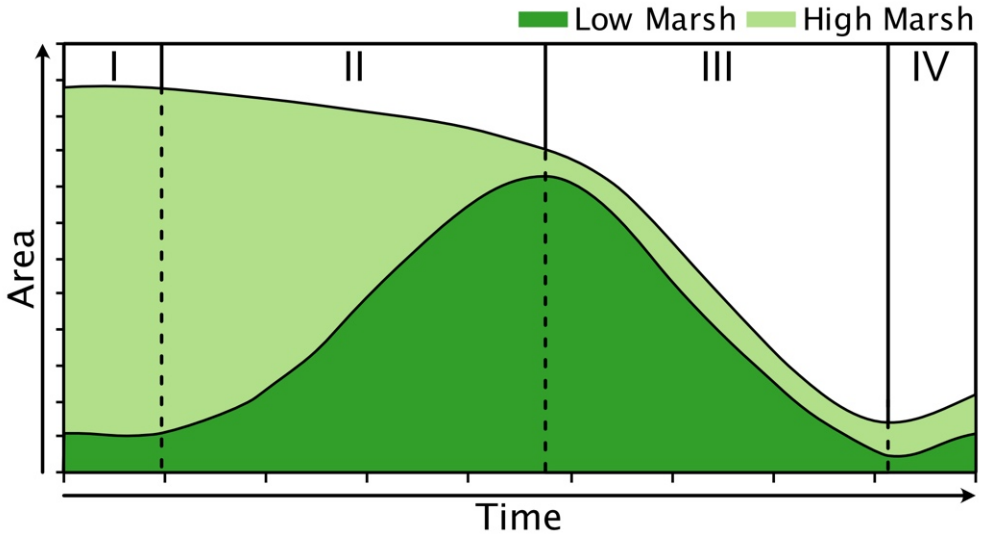

Figure 11. Schematic representation of the four identified phases associated with salt marsh area evolution in an SLR context. (**I**) Stability; (**II**) loss of maturity; (**III**) loss of area; (**IV**) recovery.

Regarding the two test areas, they have many common characteristics. However, some key differences motivate different responses to climate change, particularly, to SLR. The marsh in C. Tróia (N) is more mature than C. Tróia (S), which is reflected in the resilience to its response. Therefore, the same behavior can be observed in both sites but at different paces. The northern sector of C. Tróia is the most resilient to the consequences of SLR. Furthermore, although dunes with moderate slopes exist in both areas, the southern sector has more flattened adjacent areas, improving the ability for landward colonization of these new areas. These factors influence the pace at which each evolution phase occurs.

The above-described sequence of evolution indicates that many salt marsh areas will probably disappear in the future. However, there are landward areas adjacent to the present salt marsh limits that, in turn, will be flooded frequently enough to establish new high and low marsh areas. The increase in the annual inundation periods may also promote the deposition of sediments transported in suspension by tides, further facilitating the colonization of these supratidal areas by marsh vegetation. A consequence of these dynamics would be the formation of new salt marsh areas that may minimize (although not compensate) the projected losses in the remaining marsh or even lead to a partial recovery of the global area.

These assumptions are valid if there is no direct anthropogenic destruction of marsh areas until the end of the century and if there is a constant flux of sedimentation. However, this is not necessarily true, because these environments are increasingly threatened by anthropogenic factors and sediment deficits [80]. In addition, it is also assumed that the increase in storm intensity in the future [81,82] will not increase the impact on these areas, which is likely true for the tested marshes, since they occur in a very sheltered area.

8. Conclusions

The SMRM is a reduced complexity model that aims to compromise between complex models and simplistic approaches to quantify the evolution of salt marsh areas in a climate-change context. SMRM does not consider as many parameters as other more complex numerical and rule-based models and the number of required inputs to perform a simulation greatly simplifies the process. In fact, the results obtained with SMRM are quite similar to those obtained with SLAMM. The use of only four parameters makes

its application as universal as possible, allowing comparing the results among several environments in different places.

The sensitivity analysis showed that the most relevant parameter to the results (global area change and inundation area) is the SLR. Accretion rates also significantly impact the variation in the total area. However, their influence is not proportional to their value and does not affect the inundation area. This observation supports applying the same accretion rates for more than one study area if they are close enough to each other and have common characteristics. Finally, the RMSE of the DTM causes a variation in the results, which is approximately proportional to the error's size.

In conclusion, there are four critical parameters to consider in order to estimate the evolution of salt marsh areas until the end of the present century: (1) SLR, (2) accretion rates, (3) the morphology of each salt marsh (heights and maturity), and (4) the availability of colonizable landward space. SMRM is presented in this work as a compromise between accuracy and complexity, which allows a simple way to evaluate the behavior of intertidal areas in the context of SLR, a fundamental analysis to address coastal risk and land management policies and practices. This work also showed that the field data (obtained through cores and monitoring equipment) could be an excellent complement to remote sensing data. Finally, the combination of these parameters from different sources allowed the establishment of a simplified model to quantify the evolution of marsh areas in the future.

The test areas seem to be resilient to moderate SLR scenarios, particularly in the first half of the century (losses between 1 and 7% in the area until 2050, except for NOAA Extreme SLR scenario, with losses of 36%). Only in the second half of the century will the survival of these areas be compromised (losses between 15 and 67% in the area until 2100). Combining the results of the test areas and the sensitivity analysis, it is also possible to assume that marsh areas could positively respond to SLR if conservative scenarios were considered and if there is sediment available to compensate for the SLR. Four evolution phases were identified in these environments: stability, loss of maturity, loss of area, and recovery.

Author Contributions: Conceptualization, M.I. and M.C.F.; data curation, M.I. and A.G.C.; formal analysis, M.I., M.C.F., A.G.C. and C.A. (Carlos Antunes); funding acquisition, M.C.F. and M.L.; investigation, M.I., M.C.F., A.G.C., M.L., V.L., C.A. (César Andrade) and T.A.S.; methodology, M.I.; project administration, M.C.F. and M.L.; resources, M.C.F., A.G.C., C.A. (Carlos Antunes), M.L., V.L. and T.A.S.; software, M.I.; supervision, M.C.F.; validation, M.I. and M.C.F.; visualization, M.I.; writing—original draft, M.I., M.C.F., A.G.C., C.A. (Carlos Antunes) and M.L.; writing—review and editing, M.I., M.C.F., A.G.C., M.L., V.L. and C.A. (César Andrade). All authors have read and agreed to the published version of the manuscript.

Funding: This work was funded by the Portuguese Fundação para a Ciência e a Tecnologia (FCT) I.P./MCTES through national funds (PIDDAC)—UIDB/50019/2020, PTDC/CTA-GEO/28412/2017 (CLIMARES) and Ph.D. Grants PD/BD/142781/2018 and PD/BD/106074/2015.

Data Availability Statement: The data presented in this study are openly available in FigShare at https://doi.org/10.6084/m9.figshare.20254425.v1, reference number [65].

Conflicts of Interest: The authors declare no conflict of interest.

Appendix A. DTM and SLR

Table A1. Statistical parameters of high marsh, low marsh, and tidal flat heights for C. Tróia (N) and C. Tróia (S), considering DGPS and DTM.

Parameters	C. Tróia (N)						C. Tróia (S)					
	High Marsh		Low Marsh		Tidal Flat		High Marsh		Low Marsh		Tidal Flat	
	DGPS	DTM	DGPS	DTM	DGPS	DTM	DGPS	DTM	DGPS	DTM	DGPS	DTM
Min. (m)	1.05	0.77	0.66	0.42	−0.04	0.09	0.91	0.58	0.50	0.40	−0.21	−0.38
Q1 (m)	1.28	1.35	0.94	0.91	0.48	0.38	1.14	1.27	0.91	0.89	0.48	0.52
Median (m)	1.39	1.47	1.02	1.00	0.57	0.48	1.21	1.42	0.99	1.05	0.54	0.67
Q3 (m)	1.46	1.55	1.08	1.12	0.66	0.61	1.31	1.54	1.05	1.14	0.62	0.92
Max. (m)	1.76	1.77	1.31	1.42	0.96	1.04	1.85	2.13	1.21	1.53	1.29	1.69
IQR (m)	0.19	0.20	0.15	0.22	0.18	0.23	0.17	0.27	0.14	0.25	0.14	0.40
Mean (m)	1.37	1.43	1.00	1.00	0.57	0.52	1.24	1.40	0.97	1.01	0.57	0.74
Points	678		928		238		489		191		198	

Table A2. SLR rates for 2020, acceleration and SLR values for 2050 and 2100 for the considered SLR scenarios: IPCC RCP2.6/RCP4.5/RCP8.5, MOD.FC_2b, and NOAA Extreme.

SLR Scenario	Rate 2020	Acceleration	SLR (cm)	
	mm/year	mm/year^2	2050	2100
IPCC RCP2.6	4.463	0.000	33	55
IPCC RCP4.5	4.449	0.030	35	65
IPCC RCP8.5	4.340	0.097	37	86
MOD.FC_2b	5.260	0.152	43	111
NOAA Extreme	9.506	0.505	74	261

Appendix B. Accretion Rates

Sediment cores were collected in 2016 in the high marsh, low marsh, and tidal flat of C. Tróia (N) using a *Wan der Horst* sampler. The location of the cores was surveyed using a DGPS RTK Leica Viva NetRover GS08. No signs of significant surface mixing or bioturbation were observed during visual description. Additionally, preliminary results of the sedimentary analysis showed that the upper sediments were nearly uniform in physical properties. The sediment cores were sub-sampled every centimeter. Between 18 and 22 samples were chosen from the top 50 cm of each core for ^{210}Pb and ^{137}Cs determination. ^{210}Pb and ^{137}Cs activity profiles were obtained using a HPGe well gamma spectrometer (Ortec EG&G) measuring gamma emissions at 46.5 and 662 keV, respectively, at the Department F.-A. Forel of the University of Geneva, Switzerland. Prior to ^{210}Pb analysis, 4 samples were sealed to prevent any loss of ^{222}Rn and stored for a period of 3 weeks to ensure secular equilibrium between ^{226}Ra and ^{214}Pb. Excess ^{210}Pb was calculated as the difference between the total ^{210}Pb and the supported ^{210}Pb determined by ^{214}Pb measurement [83]. The detection efficiency of the radioisotopes was corrected for geometry. ^{210}Pb ages were calculated using the Constant Flux–Constant Sedimentation Rate model (CFCS) [83,84].

The negative values of $^{210}Pb_{excess}$ were discarded, the natural logarithmic was applied to the remaining values, and the results were plotted against depth. The slope of the line that best fits these points was used to calculate the sedimentation rate (Sr) according to the equation $Sr = -\lambda/b$, which relates the slope of line (b) with the known radioactive decay coefficient (λ).

In the ^{137}Cs profiles, the beginning of activity represents the earliest measurable fallout from the atmosphere of this artificial radionuclide (1954) and the peak in activity corresponds to the maximum atmospheric nuclear testing (1963). The sedimentation rates can be derived from the depth at which we found each of these horizons.

The profiles of the $^{210}Pb_{total}$ activity (A), the Ln $^{210}Pb_{excess}$ activity (B), and ^{137}Cs activity (C) of the cores collected in the high marsh, low marsh, and tidal flat are shown in Figures A1–A3, respectively.

None of the $^{210}Pb_{total}$ profiles show clear signs of near-surface mixing; thus, no values were excluded from the dataset. The profile of the tidal flat core (Figure A3) shows some variation between 8 and 18 cm depths, which might indicate some mixing or input of external sediments in the past. However, as it is not possible to establish distinct layers, the entire profile is used to determine the sedimentation rate. All Ln $^{210}Pb_{excess}$ profiles have a good fit of linear regression. However, the best fit is in the low marsh profile (R^2 = 0.8148).

The biggest differences are observed in the ^{137}Cs profiles. The profile of the high marsh (Figure A1) has a single, very distinctive peak at 15.5 cm, while the low marsh peak is elongated (Figure A2), indicating downward movement of the radionuclide. The ^{137}Cs profile of the tidal flat core (Figure A3) shows two distinct peaks. The existence of the second peak at 8.5 cm suggests an input of foreign, older sediments, possibly from the surrounding marsh.

The sedimentation rates obtained for each core using the methods described are presented in Table A3. All results are within the same range and are consistent between methods. There is very little difference between the sedimentation rates established for the high and low marsh cores; the biggest difference is found in the tidal flat, which is consistent with this area being the most dynamic.

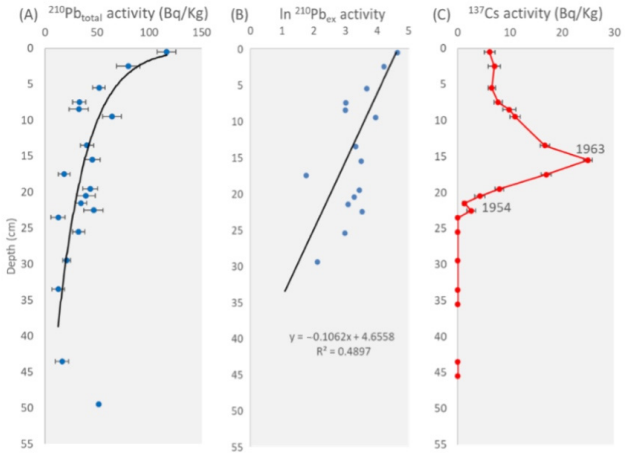

Figure A1. Profiles of the $^{210}Pb_{total}$ activity (**A**), the Ln $^{210}Pb_{excess}$ activity (**B**), and ^{137}Cs activity (**C**) of the high marsh core.

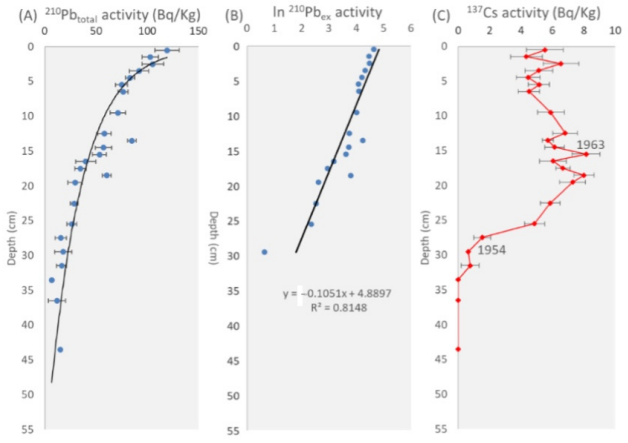

Figure A2. Profiles of the $^{210}Pb_{total}$ activity (**A**), the Ln $^{210}Pb_{excess}$ activity (**B**), and ^{137}Cs activity (**C**) of the low marsh core.

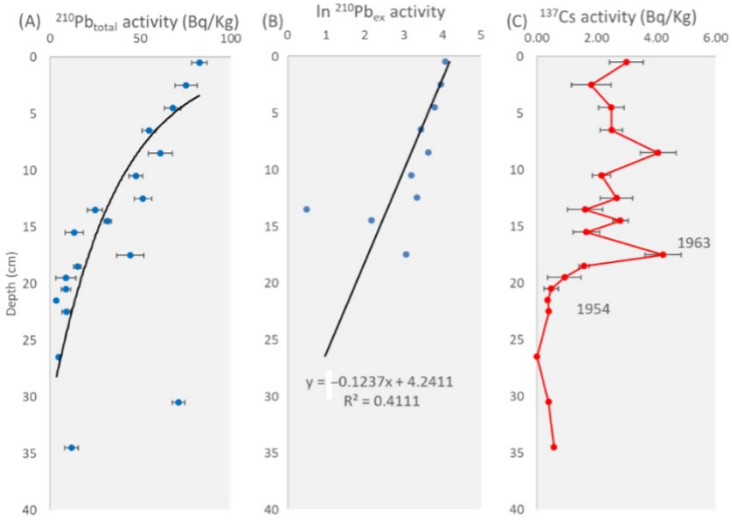

Figure A3. Profiles of the $^{210}Pb_{total}$ activity (**A**), the Ln $^{210}Pb_{excess}$ activity (**B**), and ^{137}Cs activity (**C**) of the tidal flat core.

Table A3. Sedimentation rates derived from ^{210}Pb and ^{137}Cs data for each sediment core.

Method	Reference Year	High Marsh	Low Marsh	Tidal Flat
210Pb	-	2.9 mm/year	3.0 mm/year	2.5 mm/year
137Cs	1963	2.9 mm/year	2.9 mm/year	3.3 mm/year
	1954	3.3 mm/year	4.4 mm/year	3.6 mm/year

References

1. Vernberg, F.G. Salt-marsh processes: A review. *Environ. Toxicol. Chem.* **1993**, *12*, 2167–2195. [CrossRef]
2. McLeod, E.; Chmura, G.L.; Bouillon, S.; Salm, R.; Björk, M.; Duarte, C.M.; Lovelock, C.E.; Schlesinger, W.H.; Silliman, B.R. A blueprint for blue carbon: Toward an improved understanding of the role of vegetated coastal habitats in sequestering CO_2. *Front. Ecol. Environ.* **2011**, *9*, 552–560. [CrossRef]
3. Boorman, L.A. Salt marshes—Present functioning and future change. *Mangroves Salt Marshes* **1999**, *3*, 227–241. [CrossRef]
4. Davy, A.J. Life on the edge: Saltmarshes ancient and modern. *Trans. Norfolk Norwich Nat. Soc.* **2009**, *42*, 1–10.
5. Valentim, J.M.; Vaz, N.; Silva, H.; Duarte, B.; Caçador, I.; Dias, J.M. Tagus estuary and Ria de Aveiro salt marsh dynamics and the impact of sea level rise. *Estuar. Coast. Shelf Sci.* **2013**, *130*, 138–151. [CrossRef]
6. Fagherazzi, S.; Kirwan, M.L.; Mudd, S.M.; Guntenspergen, G.R.; Temmerman, S.; D'Alpaos, A.; van del Koppel, J.; Rybczyk, J.M.; Reyes, E.; Craft, C.; et al. Numerical models of salt marsh evolution: Ecological, geomorphic, and climatic factors. *Rev. Geophys.* **2012**, *50*, RG1002. [CrossRef]
7. Bouma, T.J.; van Belzen, J.; Balke, T.; van Dalen, J.; Klaassen, P.; Hartog, A.M.; Callaghan, D.P.; Hu, Z.; Stive, M.J.F.; Temmerman, S.; et al. Short-term mudflat dynamics drive long-term cyclic salt marsh dynamics. *Limnol. Oceanogr.* **2016**, *61*, 2261–2275. [CrossRef]
8. Klemas, V. Remote Sensing of Wetlands: Case Studies Comparing Practical Techniques. *J. Coast. Res.* **2011**, *27*, 418–427. [CrossRef]
9. Shanmugam, P. Remote Sensing of the Coastal Ecosystems. *J. Geophys. Remote Sens. S* **2013**, *2*, 2169–2249. [CrossRef]
10. Hardisky, M.A.; Gross, M.F.; Klemas, V. Remote Sensing of Coastal Wetlands: Landsat TM, SPOT, and imaging spectrometers will enhance remote sensing research on wetlands. *BioScience* **1986**, *36*, 453–460. [CrossRef]
11. Goldsmith, S.B.; Eon, R.S.; Lapszynski, C.S.; Badura, G.P.; Osgood, D.T.; Bachmann, C.M.; Tyler, A.C. Assessing Salt Marsh Vulnerability Using High-Resolution Hyperspectral Imagery. *Remote Sens.* **2020**, *12*, 2938. [CrossRef]
12. Doughty, C.L.; Cavanaugh, K.C. Mapping Coastal Wetland Biomass from High Resolution Unmanned Aerial Vehicle (UAV) Imagery. *Remote Sens.* **2019**, *11*, 540. [CrossRef]
13. Oteman, B.; Morris, E.P.; Peralta, G.; Bouma, T.J.; van der Wal, D. Using Remote Sensing to Identify Drivers behind Spatial Patterns in the Bio-physical Properties of a Saltmarsh Pioneer. *Remote Sens.* **2019**, *11*, 511. [CrossRef]
14. Lamb, B.T.; Tzortziou, M.A.; McDonald, K.C. Evaluation of Approaches for Mapping Tidal Wetlands of the Chesapeake and Delaware Bays. *Remote Sens.* **2019**, *11*, 2366. [CrossRef]
15. Pendleton, L.; Donato, D.C.; Murray, B.C.; Crooks, S.; Jenkins, W.A.; Sifleet, S.; Craft, C.; Fourqurean, J.W.; Kauffman, J.B.; Marbà, N.; et al. Estimating global "Blue Carbon" emissions from conversion and degradation of vegetated coastal ecosystems. *PLoS ONE* **2012**, *7*, e43542. [CrossRef]
16. Laffoley, D.; Grimsditch, G.D. *The Management of Natural Coastal Carbon Sinks*; IUCN Technical Report; IUCN: Gland, Switzerland, 2009.

17. Luisetti, T.; Jackson, E.L.; Turner, R.K. Valuing the European "coastal blue carbon" storage benefit. *Mar. Pollut. Bull.* **2013**, *71*, 101–106. [CrossRef]
18. Townend, I.; Rossington, K.; Knaapen, M.A.F.; Richardson, S. The dynamics of intertidal mudflats and saltmarshes within estuaries. In Proceedings of the Coastal Engineering Conference, Shanghai, China, 30 June–5 July 2010; Smith, J.M., Lynett, P., Eds.; Coastal Engineering Research Council: Reston, VA, USA, 2010; Volume 32, pp. 1–10.
19. IPCC. Climate Change 2014: Impacts, Adaptation, and Vulnerability—Part A: Global and Sectoral Aspects. In *Contribution of Working Group II to the Fifth Assessment Report of the Intergovernmental Panel on Climate Change*; Field, C.B., Barros, V.R., Dokken, D.J., Mach, K.J., Mastrandrea, M.D., Bilir, T.E., Chatterjee, M., Ebi, K.L., Estrada, Y.O., Genova, R.C., et al., Eds.; Cambridge University Press: Cambridge, UK; New York, NY, USA, 2014; p. 1132.
20. Kirwan, M.L.; Megonigal, J.P. Tidal wetland stability in the face of human impacts and sea-level rise. *Nature* **2013**, *504*, 53–60. [CrossRef]
21. Constanza, R.; Voinov, A. (Eds.) *Landscape Simulation Modeling: A Spatially Explicit Dynamic Approach*; Springer: Berlin/Heidelberg, Germany, 2004. [CrossRef]
22. Morris, J.T.; Sundareshwar, P.V.; Nietch, C.T.; Kjerfve, B.; Cahoon, D.R. Responses of coastal wetlands to rising sea level. *Ecology* **2002**, *83*, 2869–2877. [CrossRef]
23. Fagherazzi, S.; Hannion, M.; D'Odorico, P. Geomorphic structure of tidal hydrodynamics in salt marsh creeks. *Water Resour. Res.* **2008**, *44*, W02419. [CrossRef]
24. Raposa, K.B.; Wasson, K.; Smith, E.; Crooks, J.A.; Delgado, P.; Fernald, S.H.; Ferner, M.C.; Helms, A.; Hice, L.A.; Mora, J.W.; et al. Assessing tidal marsh resilience to sea-level rise at broad geographic scales with multi-metric indices. *Biol. Conserv.* **2016**, *204*, 263–275. [CrossRef]
25. Best, S.N.; Van der Wegen, M.; Dijkstra, J.; Willemsen, P.W.J.M.; Borsje, B.W.; Roelvink, D.J.A. Do salt marshes survive sea level rise? Modelling wave action, morphodynamics and vegetation dynamics. *Environ. Model. Softw.* **2018**, *109*, 152–166. [CrossRef]
26. Paola, C.; Leeder, M. Environmental Dynamics: Simplicity versus complexity. *Nature* **2011**, *469*, 38–39. [CrossRef] [PubMed]
27. Murray, A.B. Contrasting the goals, strategies and predictions associated with simplified numerical models and detailed simulations. *Predict. Geomorphol.* **2003**, *135*, 151–165. [CrossRef]
28. French, J.; Payo, A.; Murray, B.; Orford, J.; Eliot, M.; Cowell, P. Appropriate complexity for the prediction of coastal and estuarine geomorphic behaviour at decadal to centennial scales. *Geomorphology* **2016**, *256*, 3–16. [CrossRef]
29. Silva, A.N.; Taborda, R.; Andrade, C.; Ribeiro, M. The future of insular beaches: Insights from a past-to-future sediment budget approach. *Sci. Total Environ.* **2019**, *676*, 692–705. [CrossRef]
30. Silva, M.; Patrício, P.; Mariano, A.; Morais, M.; Valério, M. Obtenção de Dados LiDAR para as Zonas Costeiras de Portugal Continental. *Segundas Jorn. Eng. Hidrográfica* **2012**, *2*, 19–22.
31. Andrade, C.; Pires, H.O.; Taborda, R.; Freitas, M.C. Zonas Costeiras. In *Alterações Climáticas em Portugal. Cenários, Impactos e Medidas de Adaptação. Projecto SIAM II*, 1st ed.; Santos, F.D., Miranda, P., Eds.; Gradiva: Lisboa, Portugal, 2006; pp. 169–208.
32. ICNB. Plano Setorial da Rede Natura 2000—1130 Estuários. Instituto da Conservação da Natureza e da Biodiversidade, 2008. Available online: http://www2.icnf.pt/portal/pn/biodiversidade/rn2000/resource/doc/rn-plan-set/hab/hab-1130 (accessed on 1 December 2021).
33. EEA. Report under the Article 17 of the habitats Directive—Period 2007–2012. 1130 Estuaries. European Environment Agency, 2013. Available online: https://forum.eionet.europa.eu/habitat-art17report/library/2007-2012-reporting/factsheets/habitats/coastal-habitats/1130-estuaries/download/en/1/1130-estuaries.pdf (accessed on 1 December 2021).
34. Guerreiro, V.; Bettencourt, P.; Santos, A. Avaliação de Impactes Ambientais em Sistemas Estuarinos: Revisão de Estudos de Caso nos Estuários do Sado, Mira e Ria Formosa. In *Actas do 1.º Simpósio Interdisciplinar de Processos Estuarinos*; Universidade do Algarve: Faro, Portugal, 1998.
35. Bettencourt, A.; Gomes, V.; Dias, A.; Ferreira, G.; Silva, M.; Costa, L. *Estuários Portugueses*; Direcção dos Serviços de Planeamento, Instituto da Água, Ministério das Cidades, Ordenamento do Território e Ambiente: Lisboa, Portugal, 2003.
36. Dias, A.A. Estuário do Sado. In *Encontro com o Sado*; Escola Superior de Educação de Setúbal: Setúbal, Portugal, April 1999; pp. 13–26.
37. Loureiro, J.M. *Monografias Hidrológicas dos Principais Cursos de água de Portugal Continental*; Direcção-Geral dos Recursos e Aproveitamentos Hidráulicos: Lisboa, Portugal, 1986.
38. Moreira, M.E.S.A. Recent Saltmarsh Changes and Sedimentation Rates in the Sado Estuary, Portugal. *J. Coast. Res.* **1992**, *8*, 631–640. Available online: https://www.jstor.org/stable/4298012 (accessed on 1 December 2021).
39. Ambar, I.; Fiúza, A.F.G.; Sousa, F.M.; Lourenço, I.O. General circulation in the lower Sado estuary under drought conditions. In Proceedings of the Actual Problems of Oceanography in Portugal, Lisboa, Portugal, 20–21 November 1980; JNICT/NATO: Lisboa, Portugal, 1982; pp. 97–107.
40. Neves, R.J.; Ferreira, J.N.R. *Modelo Matemático do Estuário do Sado, Extensão à plataforma Costeira Adjacente*; Ed Serviço Nacional de Parques e Reservas e Conservação da Natureza: Lisboa, Portugal, 1987.
41. Costas, S.; Rebêlo, L.; Brito, P.; Burbidge, C.I.; Prudêncio, M.I.; FitzGerald, D. The Joint History of Tróia Peninsula and Sado Ebb-Delta. In *Sand and Gravel Spits. Coastal Research Library*; Randazzo, G., Jackson, D.W.T., Cooper, J.A.G., Eds.; Springer International Publishing: Basel, Switzerland, 2015; p. 25. [CrossRef]
42. Davis, R.A.; FitzGerald, D.M. *Beaches and Coasts*; Blackwell Publishing Company: Hoboken, NJ, USA, 2004. [CrossRef]
43. *MATLAB*; 9.4.0.813654 (R2018a); The MathWorks Inc.: Natick, MA, USA, 2018.

44. *MATLAB*; 9.8.0.1380330 (R2020a); The MathWorks Inc.: Natick, MA, USA, 2020.
45. ESRI. *ArcGIS Pro*; Release 2.6.0; Environmental Systems Research Institute: Redlands, CA, USA, 2020.
46. Inácio, M.; Freitas, M.C.; Cunha, A.G.; Antunes, C.; Leira, M.; Lopes, V.; Andrade, C. SMRM. 2022. Available online: https://figshare.com/articles/software/SMRM/20237409/1 (accessed on 8 July 2022).
47. SLAMM. *SLAMM 6.7 Technical Documentation*; Sea Level Affecting Marshes Model, Version 6.7 Beta; Warren Pinnacle Consulting, Inc.: Waitsfield, VT, USA, 2016. Available online: http://warrenpinnacle.com/prof/SLAMM6/SLAMM_6.7_Technical_Documentation.pdf (accessed on 1 December 2021).
48. SLAMM. *User's Manual*; SLAMM 6.7 beta; Warren Pinnacle Consulting, Inc.: Waitsfield, VT, USA, 2016. Available online: http://warrenpinnacle.com/prof/SLAMM6/SLAMM_6.7_Users_Manual.pdf (accessed on 1 December 2021).
49. Fernandez-Nunez, M.; Burningham, H.; Díaz-Cuevas, P.; Ojeda-Zújar, J. Evaluating the Response of Mediterranean-Atlantic Saltmarshes to Sea-Level Rise. *Resources* **2019**, *8*, 50. [CrossRef]
50. Melet, A.; Meyssignac, B.; Almar, R.; Le Cozannet, G. Under-estimated wave contribution to coastal sea-level rise. *Nat. Clim. Chang.* **2018**, *8*, 234–239. [CrossRef]
51. Antunes, C. Previsão de Marés dos Portos Principais de Portugal. FCUL Webpage, 2007. Available online: http://webpages.fc.ul.pt/~{}cmantunes/hidrografia/hidro_mares.html (accessed on 1 December 2021).
52. Antunes, C. Assessment of sea level rise at West coast of Portugal mainland and its projection for the 21st century. *J. Mar. Sci. Eng.* **2019**, *7*, 61. [CrossRef]
53. Gesch, D.B. Analysis of Lidar Elevation Data for Improved Identification and Delineation of Lands Vulnerable to Sea-Level Rise. *J. Coast. Res.* **2009**, *10053*, 49–58. [CrossRef]
54. Fagherazzi, S. The ephemeral life of a salt marsh. *Geology* **2013**, *41*, 943–944. [CrossRef]
55. Maune, D.F.; Maitra, J.B.; McKay, E.J. Accuracy standards & guidelines. In *Digital Elevation Model Technologies and Applications: The DEM Users Manual*, 2nd ed.; Maune, D., Ed.; American Society for Photogrammetry and Remote Sensing: Bethesda, MD, USA, 2007; pp. 65–97.
56. Mendes, V.; Barbosa, S.; Carinhas, D. Vertical land motion in the Iberian Atlantic coast and its implication for sea level change evaluation. *J. Appl. Geod.* **2020**, *14*, 361–378. [CrossRef]
57. Hammond, W.; Blewitt, G.; Kreemer, C.; Nerem, R. GPS Imaging of Global Vertical Land Motion for Studies of Sea Level Rise. *J. Geophys. Res. Solid Earth* **2021**, *126*, e2021JB022355. [CrossRef]
58. IPCC. Climate Change 2013: The Physical Science Basis. In *Contribution of Working Group I to the Fifth Assessment Report of the Intergovernmental Panel on Climate Change*; Stocker, T.F., Qin, D., Plattner, G.K., Tignor, M., Allen, S.K., Boschung, J., Nauels, A., Xia, Y., Bex, V., Midgley, P.M., Eds.; Cambridge University Press: Cambridge, UK; New York, NY, USA, 2013; p. 1535.
59. Sweet, V.W.; Kopp, R.E.; Weaver, P.C.; Obeysekera, J.; Horton, M.H.; Thiele, E.R.; Zervas, C. *Global and Regional Sea Level Rise Scenarios for the United States*; NOAA Technical Report NOS CO-OPS 083; National Oceanic and Atmospheric Admin: Washington, DC, USA, 2017.
60. IPCC. Climate Change 2021: The Physical Science Basis. In *Contribution of Working Group I to the Sixth Assessment Report of the Intergovernmental Panel on Climate Change*; Masson-Delmotte, V., Zhai, P., Pirani, A., Connors, S.L., Péan, C., Berger, S., Caud, N., Chen, Y., Goldfarb, L., Gomis, M.I., et al., Eds.; Cambridge University Press: Cambridge, UK; New York, NY, USA, 2021; *in press*. [CrossRef]
61. IPCC. Climate Change 2007: Synthesis Report. In *Contribution of Working Groups I, II and III to the Fourth Assessment Report of the Intergovernmental Panel on Climate Change*; Core Writing Team, Pachauri, R.K., Reisinger, A., Eds.; IPCC: Geneva, Switzerland, 2007; p. 104.
62. Fagherazzi, S.; Mariotti, G.; Leonardi, N.; Canestrelli, A.; Nardin, W.; Kearney, W.S. Salt Marsh Dynamics in a Period of Accelerated Sea Level Rise. *J. Geophys. Res. Earth Surf.* **2020**, *125*, e2019JF005200. [CrossRef]
63. Nolte, S.; Koppenaal, E.C.; Esselink, P.; Dijkema, K.S.; Schuerch, M.; De Groot, A.V.; Bakker, J.P.; Temmerman, S. Measuring sedimentation in tidal marshes: A review on methods and their application in biogeomorphological studies. *J. Coast. Conserv.* **2013**, *17*, 301–325. [CrossRef]
64. Freitas, M.C.; Andrade, C.; Cruces, A.; Munhá, J.; Sousa, M.J.; Moreira, S.; Jouanneau, J.M.; Martins, L. Anthropogenic influence in the Sado Estuary (Portugal): A geochemical approach. *J. Iber. Geol.* **2008**, *34*, 271–286.
65. Inácio, M.; Freitas, M.C.; Cunha, A.G.; Antunes, C.; Leira, M.; Lopes, V.; Andrade, C.C. Tróia (N) and (S) SMRM and SLAMM results 2022. Available online: https://figshare.com/articles/dataset/C_Tr_ia_N_and_S_SMRM_and_SLAMM_results/20254425/1 (accessed on 8 July 2022).
66. Scardino, G.; Sabatier, F.; Scicchitano, G.; Piscitelli, A.; Milella, M.; Vecchio, A.; Anzidei, M.; Mastronuzzi, G. Sea-Level Rise and Shoreline Changes Along an Open Sandy Coast: Case Study of Gulf of Taranto, Italy. *Water* **2020**, *12*, 1414. [CrossRef]
67. Anzidei, M.; Scicchitano, G.; Scardino, G.; Bignami, C.; Tolomei, C.; Vecchio, A.; Serpelloni, E.; De Santis, V.; Monaco, C.; Milella, M.; et al. Relative Sea-Level Rise Scenario for 2100 along the Coast of South Eastern Sicily (Italy) by InSAR Data, Satellite Images and High-Resolution Topography. *Remote Sens.* **2021**, *13*, 1108. [CrossRef]
68. Gesch, D.B. Consideration of Vertical Uncertainty in Elevation-Based Sea-Level Rise Assessments: Mobile Bay, Alabama Case Study. *J. Coast. Res.* **2013**, *63*, 197–210. [CrossRef]
69. Gesch, D.B. Best Practices for Elevation-Based Assessments of Sea-Level Rise and Coastal Flooding Exposure. *Front. Earth Sci.* **2018**, *6*, 230. [CrossRef]

70. Temmerman, S.; Govers, G.; Meir, P.; Wartel, S. Modelling long-term tidal marsh growth under changing tidal conditions and suspended sediment concentrations, Scheldt Estuary, Belgium. *Mar. Geol.* **2003**, *193*, 151–159. [CrossRef]
71. Laengner, M.L.; Siteur, K.; van der Wal, D. Trends in the Seaward Extent of Saltmarshes across Europe from Long-Term Satellite Data. *Remote Sens.* **2019**, *11*, 1653. [CrossRef]
72. Belliard, J.P.; Di Marco, N.; Carniello, L.; Toffolon, M. Sediment and vegetation spatial dynamics facing sea-level rise in microtidal salt marshes: Insights from an ecogeomorphic model. *Adv. Water Resour.* **2016**, *93*, 249–264. [CrossRef]
73. Kirwan, M.L.; Temmerman, S.; Skeehan, E.E.; Guntenspergen, G.R.; Fagherazzi, S. Overestimation of marsh vulnerability to sea level rise. *Nat. Clim. Chang.* **2016**, *6*, 253–260. [CrossRef]
74. Crosby, S.C.; Sax, D.F.; Palmer, M.E.; Booth, H.S.; Deegan, L.A.; Bertness, M.D.; Leslie, H.M. Salt marsh persistence in threatened by predicted sea-level rise. *Estuar. Coast. Shelf Sci.* **2016**, *181*, 93–99. [CrossRef]
75. Schuerch, M.; Spencer, T.; Temmerman, S.; Kirwan, M.L.; Wolff, C.; Lincke, D.; McOwen, C.J.; Pickering, M.D.; Reef, R.; Vafeidis, A.T.; et al. Future response of global coastal wetlands to sea-level rise. *Nature* **2018**, *561*, 231–234. [CrossRef]
76. Giuliani, S.; Bellucci, L. Salt Marshes: Their Role in Our Society and Threats Posed to Their Existence. In *World Seas: An Environmental Evaluation*; Sheppard, C., Ed.; Academic Press: Cambridge, MA, USA, 2019; pp. 79–101. [CrossRef]
77. Macreadie, P.I.; Costa, M.D.P.; Atwood, T.B.; Friess, D.A.; Kelleway, J.J.; Kennedy, H.; Lovelock, C.E.; Serrano, O.; Fuarte, C.M. Blue carbon as a natural climate solution. *Nat. Rev. Earth Environ.* **2021**, *2*, 826–839. [CrossRef]
78. Howard, J.; Sutton-Grier, A.; Herr, D.; Kleypas, J.; Landis, E.; Mcleod, E.; Pidgeon, E.; Simpson, S. Clarifying the role of coastal and marine systems in climate mitigation. *Front. Ecol. Environ.* **2017**, *15*, 42–50. [CrossRef]
79. Duarte, B.; Carreiras, J.; Caçador, I. Climate Change Impacts on Salt Marsh Blue Carbon, Nitrogen and Phosphorous Stocks and Ecosystem Services. *Appl. Sci.* **2021**, *11*, 1969. [CrossRef]
80. Farris, A.S.; Defne, Z.; Ganju, N.K. Identifying Salt Marsh Shorelines from Remotely Sensed Elevation Data and Imagery. *Remote Sens.* **2019**, *11*, 1795. [CrossRef]
81. Giorgi, F.; Lionello, P. Climate change projections for the Mediterranean region. *Glob. Planet. Chang.* **2007**, *63*, 90–104. [CrossRef]
82. Lionello, P.; Özsoy, E.; Planton, S.; Zanchetta, G. Climate Variability and Change in the Mediterranean Region. *Glob. Planet. Chang.* **2017**, *151*, 1–3. [CrossRef]
83. Appleby, P.G. Chronostratigraphic techniques in recent sediments. In *Tracking Environmental Change Using Lake Sediments Volume 1: Basin Analysis, Coring, and Chronological Techniques*; Last, W.M., Smol, J.P., Eds.; Kluwer Academic: Dordrecht, The Netherlands, 2001; pp. 171–203.
84. Sanchez-Cabeza, J.A.; Ruiz-Fernández, A.C. 210Pb sediment radiochronology: An integrated formulation and classification of dating models. *Geochim. Cosmochim.* **2012**, *82*, 183–200. [CrossRef]